INTERNATIONAL GEOLOGY REVIEW
https://doi.org/10.1080/00206814.2025.2612208

Taylor & Francis
Taylor & Francis Group

From subduction initiation to oceanic core complex formation: a tale of two ophiolites in the Kurdistan, NW Iran

Bahman Rahimzadeh[a], Fatemeh Sepidbar[b], Harald Furnes[c] and Richard M. Palin[d]

[a]Department of Geology, Faculty of Earth Sciences, Shahid Beheshti University, Tehran, Iran; [b]Department of Geology, Faculty of Science, Ferdowsi University of Mashhad, Mashhad, Iran; [c]Department of Earth Science, University of Bergen Bergen, Norway; [d]Department of Earth Sciences, University of Oxford, Oxford, UK

ABSTRACT

The processes of subduction initiation and oceanic core complex (OCC) formation are essential to understanding plate tectonic evolution. The Kermanshah–Walash Ophiolitic Complex (KWOC) in Kurdistan, NW Iran, preserves a unique record of both mechanisms in spatially parallel but temporally distinct Late Cretaceous (Razab) and Eocene (Sarv-Abad) ophiolites. These ophiolites comprise peridotite, gabbroic bodies, a dike complex, and pillowed and massive basaltic lavas. Whole-rock geochemistry, U–Pb zircon geochronology, and field structures reveal distinct ages and tectonic settings for the two ophiolites. While radiolarian cherts constrain the Razab ophiolite to the Cretaceous, new U–Pb zircon (42–38 Ma) geochronology firmly places the formation of the Sarv-Abad oceanic core complex in the Eocene. The Cretaceous Razab unit contains high-Cr# spinel chromitite (0.77–0.82), forearc, and island arc tholeiitic (IAT) lavas, supporting formation during subduction initiation. In contrast, the Eocene Sarv-Abad unit features mylonitized gabbros, syn-extensional dikes, and contemporaneous D-MORB/E-MORB magmatism derived from heterogeneous mantle melting, diagnostic of an Oceanic Core Complex (OCC) in an extensional back-arc. Our results demonstrate that the KWOC was shaped by two distinct geodynamic mechanisms: subduction initiation in the Cretaceous and oceanic core complex formation in the Eocene. Despite ~50 Myr separation, both units were emplaced during the Miocene closure, suggesting how contrasting mechanisms may have shaped the KWOC. The OCC model also offers a potential resolution to prior ambiguities in the geodynamic evolution of Peri-Arabic ophiolites.

ARTICLE HISTORY
Received 20 April 2025
Accepted 30 November 2025

KEYWORDS
Razab; Sarv-Abad; forearc; detachment faulting; oceanic core complex; Kermanshah-walash ophiolitic belt

1. Introduction

Ophiolites offer valuable records to study the formation and evolution of plate boundaries in a range of geodynamic settings (e.g. Moores 1983; Maruyama *et al*. 1996; Dilek and Furnes 2011, 2014; Dilek and Yang 2018; Furnes and Dilek 2022). Geochemical and geochronological data have revealed that ophiolitic crust and lithospheric mantle are not only generated at mid-ocean ridges (MORs) far from subduction zones (Rollinson 2017) but also during subduction initiation in forearc/back-arc settings (e.g. Izu–Bonin–Mariana, Tonga–Kermadec; Stern *et al*. 2012). Two spatially parallel, but temporally distinct, Late Cretaceous and Eocene–Oligocene ophiolitic and associated marine sedimentary sequences occur in the NW Zagros segment of the Peri-Arabic ophiolitic belt, a ~2000-km long orogenic belt that stretches from the East Anatolian Fault in southeastern Turkey and continues through NW Iraq–NW Iran (Agard *et al*. 2007; Whitechurch *et al*. 2013; Ao *et al*. 2016; Sepidbar *et al*., 2021). To the southeast, this system continues into the distinct tectonic domain of the Makran subduction zone (Sepidbar *et al*. 2020). They are characterized as scattered ophiolite fragments, typically of limited aerial extent, with crustal ages ranging from ~90 to ~29 Ma and geochemical signatures indicating formation in an arc/back-arc within a nascent subduction zone (Whitechurch *et al*. 2013).

Peri-Arabic ophiolites include Turkish ophiolites (e.g. Pozantı-Karsantı, Mersin), the Khoy, Kermanshah (Harsin, Sahneh, Kamyaran), and Kurdistan (Razab, Sarv-Abad) of NW Iran; the Penjween, Mawat, and Hasanbag ophiolites in Iraq (Aswad *et al*. 2011); the Neyriz and Esfandagheh ophiolites in southern Iran; and the Semail (Oman) and Makran ophiolites to the southeast (Moghadam and Stern 2014). To the northwest, these units are exposed along the Iran–Iraq boundary. The Kermanshah and Kurdistan ophiolites (Iran), together with the Mawat-Hasanbag ophiolites and the predominantly volcanic-sedimentary Walash Group (Iraq), form a major tectonostratigraphic zone known as the Kermanshah–Walash Ophiolitic Complex (KWOC)

CONTACT Fatemeh Sepidbar sepidbar@um.ac.ir Department of Geology, Faculty of Science, Ferdowsi University of Mashhad, Mashhad, Iran
Supplemental data for this article can be accessed online at https://doi.org/10.1080/00206814.2025.2612208

(Ghorbani *et al*. 2022). The Kermanshah/Kurdistan region of northwestern Iran is a tectonically active area that preserves critical records of the tectonic evolution of the Neotethyan realm from the Late Mesozoic to Cenozoic. The Kermanshah and Kurdistan ophiolites (Figure 1) belong to two different domains: (i) a section of Cretaceous oceanic sequences underplated beneath the Sanandaj–Sirjan Zone and (ii) a Cenozoic arc/back-arc that formed in the Late Cretaceous oceanic crust (Ghorbani *et al*. 2022). Both the timing of the ophiolite formation and the geochemical and temporal evolution of the Kermanshah and Kurdistan ophiolites remain debated. A plagiogranitic dike in the Kermanshah ophiolite has a whole-rock K–Ar age of 86.3 ± 7.8 Ma (Delaloye and Desmons 1980), whereas U–Pb zircon data from both rodingitized gabbro of the Harsin and Sahneh-Kamyaran (Kermanshah) ophiolite have weighted mean ages of 80 Ma and 38 Ma, respectively (Ao *et al*. 2016). However, only limited radiometric age constraints are available for the Cenozoic ophiolites of Kurdistan, with K–Ar ages of the Sarv-Abad basaltic rocks ranging from 59 Ma to 29 Ma (Ghorbani *et al*. 2022). However, the geochemistry, petrogenesis, and tectonomagmatic evolution of the Cretaceous (Razab) and Eocene (Sarv-Abad) crustal sequences in Kurdistan remain poorly understood. Investigating these units can provide new insights into the Mesozoic–Cenozoic evolution of the region.

In addition, most crustal sequences are mixtures of the common occurrence of older MORB-like lavas stratigraphically beneath younger arc-like sequences (Ghorbani *et al*. 2022), alongside an incomplete understanding of the genetic relationship between depleted (D-) and enriched (E-)MORB magmas, raises key questions about magma generation in evolving subduction systems. Enriched mid-ocean ridge basalts (E-MORB) commonly erupt at mid-ocean ridge (MOR) systems and back-arc basins (BAB). However, their relationship to 'depleted' MORB (D-MORB) and the processes controlling their magmatic evolution are not fully understood, raising further general questions about magma generation in the mantle. This study investigates whether the Cretaceous Razab and Eocene Sarv-Abad ophiolites are genetically linked fragments of a single subduction system or independent entities formed by distinct geodynamic mechanisms. We evaluate these alternatives through three interconnected hypotheses: (i) Genetic linkage: This model requires the Razab ophiolite to exhibit forearc signatures from subduction

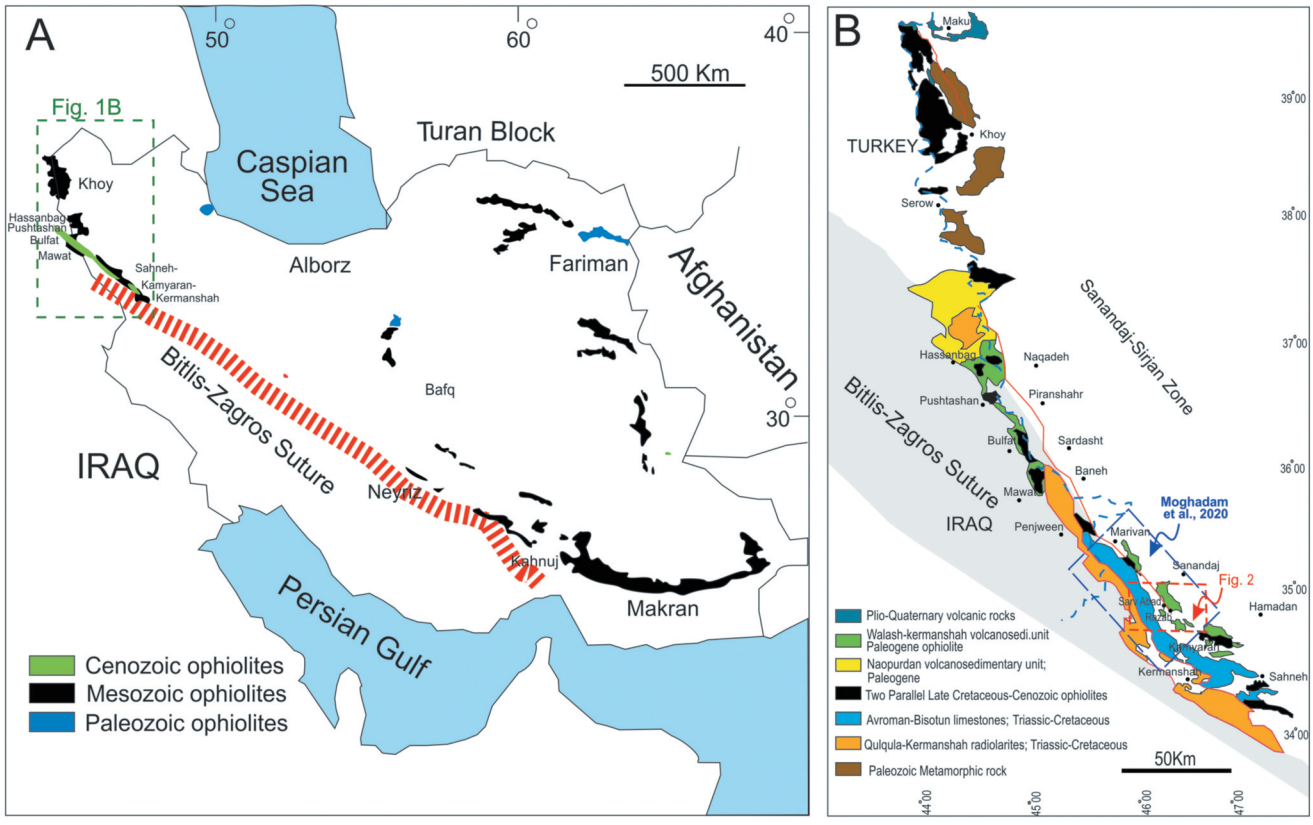

Figure 1. (A) Regional map of the Middle East, including the NW Zagros belt in the Iran–Iraq border (modified from Koshnaw *et al*. 2017); (B) basic map showing the spreading of the Kermanshah–Walash ophiolitic complex with highlighting on the Sarv-Abad ophiolite (after Ali *et al*. 2013).

initiation. The Sarv-Abad ophiolite would then show back-arc features from continued slab evolution, with both units sharing a common mantle heterogeneity. (ii) Independence: This model implies the ophiolites have fundamentally distinct origins. They would exhibit different structural architectures (obduction-related vs. detachment faulting), mantle sources (depleted SSZ vs. heterogeneous MORB), and geochemical trajectories (subduction- vs. extension-dominated). (iii) The D-MORB/E-MORB dichotomy in Sarv-Abad reflects either inherited mantle heterogeneity from the Razab system (supporting linkage) or independent mantle processes unrelated to Cretaceous subduction (supporting independence). These hypotheses are addressed via three targeted research questions: (1) Did contrasting tectonic settings (subduction initiation vs. detachment faulting) form the Razab and Sarv-Abad ophiolites, based on field structural relationships and mineral-chemical data? (2) Can Sarv-Abad's geochemical dichotomy (D-MORB vs. E-MORB) be explained by heterogeneous mantle melting rather than progressive mantle melting? (3) How does integrated U–Pb geochronology and structural analysis redefine the timing of formation and emplacement mechanisms within the KWOC tectonic model relative to prior interpretations (Saccani *et al*. 2014; Allahyari *et al*. 2014; Ao *et al*. 2016)?

Here, we report new zircon U–Pb ages, structural field relations, and geochemical data from both the Razab and Sarv-Abad segments of the Kurdistan ophiolite to more precisely constrain the formation timing of the Neo-Tethys oceanic floor and its subduction and propose a revised model for the geodynamic evolution of the Peri-Arabic ophiolitic system. Our integrated dataset supports the independence model, revealing that the Cretaceous Razab ophiolite formed during subduction initiation, while the Eocene Sarv-Abad ophiolite represents an oceanic core complex exhumed in an extensional back-arc.

2. Geological setting

2.1. General geology of the KWOC

The KWOC is a key tectonostratigraphic zone in NW Iran. This section summarizes its general geology and reviews previous work to provide context for this study. A wide variety of ultramafic-to-mafic rocks outcrop along the Peri-Arabic ophiolite belt, including the Kermanshah (Harsin, Sahneh, Kamyaran), Kurdistan (Razab, Sarv-Abad), Neyriz, and Esfandagheh ophiolites in Iran (Moghadam and Stern 2014) and the Penjween, Mawat-Hasanbag ophiolites in Iraq (Aswad *et al*. 2011). The Cretaceous Kermanshah and Eocene–Oligocene Kurdistan ophiolites in the NW Iranian KWOC outcrop within a structural window within the turbiditic phyllites of the Sanandaj–Sirjan zone (Figure 2A). Previous studies suggest a supra-subduction zone affinity for the mantle section of the Mesozoic Kermanshah ophiolite (Nouri *et al*. 2018). In the Kermanshah, and especially in the Sahneh-Kamyaran region (Ao *et al*. 2016), Palaeocene–Eocene turbidites and Eocene pillow lavas stratigraphically overlie the Late Cretaceous peridotites. The Eocene pillow lavas differ from the Late Cretaceous pillows in that they are intercalated with green shale and sandstone turbidites. Dike swarms, including early basaltic and diabasic dikes and late dacitic rhyolitic to microdioritic dikes (usually <0.5 m, but locally >1 m wide), occur in the Kermanshah region and record Eocene U–Pb zircon ages (Moghadam and Stern 2014). These dikes are interpreted to have formed during extension associated with intra-oceanic magmatism (Whitechurch *et al*. 2013). Whitechurch *et al*. (2013) suggested that the Eocene ophiolitic rocks (pillow lavas, gabbros, and dikes) were emplaced into the Late Cretaceous Kermanshah ophiolite close to the ocean–continent transition.

The Kurdistan ophiolite forms one of the mantle and crustal outcrops (~150 km^2 areal extent) of the KWOC (Figure 1A, B). It contains the same Cretaceous (Razab) and Eocene (Sarv-Abad) ophiolitic crustal sequences, separated by Sanandaj–Sirjan units. The mafic rocks exhibit tholeiitic to calc-alkaline affinities and geochemical signatures that range from depleted (D-MORB) to enriched (E-MORB) types, similar to those reported from the Sahneh-Kamyaran area (Ao *et al*. 2016). A geochronological study of Sarv-Abad lavas showed different ages of Palaeocene–Eocene (59–52 Ma) and Oligocene (29 Ma) for the light rare earth element (LREE)-depleted and LREE-enriched lava, respectively (Ghorbani *et al*. 2022). These authors considered the Sarv-Abad volcanic rocks as a Palaeocene immature and Oligocene mature back-arc basin along the Eurasian continental margin that ultimately accreted to the Eurasian continent following the Early Palaeocene Ocean closure (Arvin and Robinson 1994; Moghadam 2009) and continental collision. In contrast, no detailed work has been performed on the geology and petrogenesis of Cretaceous ophiolites, Eocene gabbros, or plagiogranites. Here, we study major and trace element variations in selected samples from both Cretaceous and Eocene Kurdistan ophiolite occurrences within the KWOC, highlighting their ages by U–Pb dating and genesis from geochemistry, and elucidate their mechanisms and conditions of formation.

2.2. Geology of the Kurdistan ophiolite

Prior investigation of the Kurdistan ophiolite has defined four main units (Figure 2; e.g. Braud 1987): (i) Sanandaj–

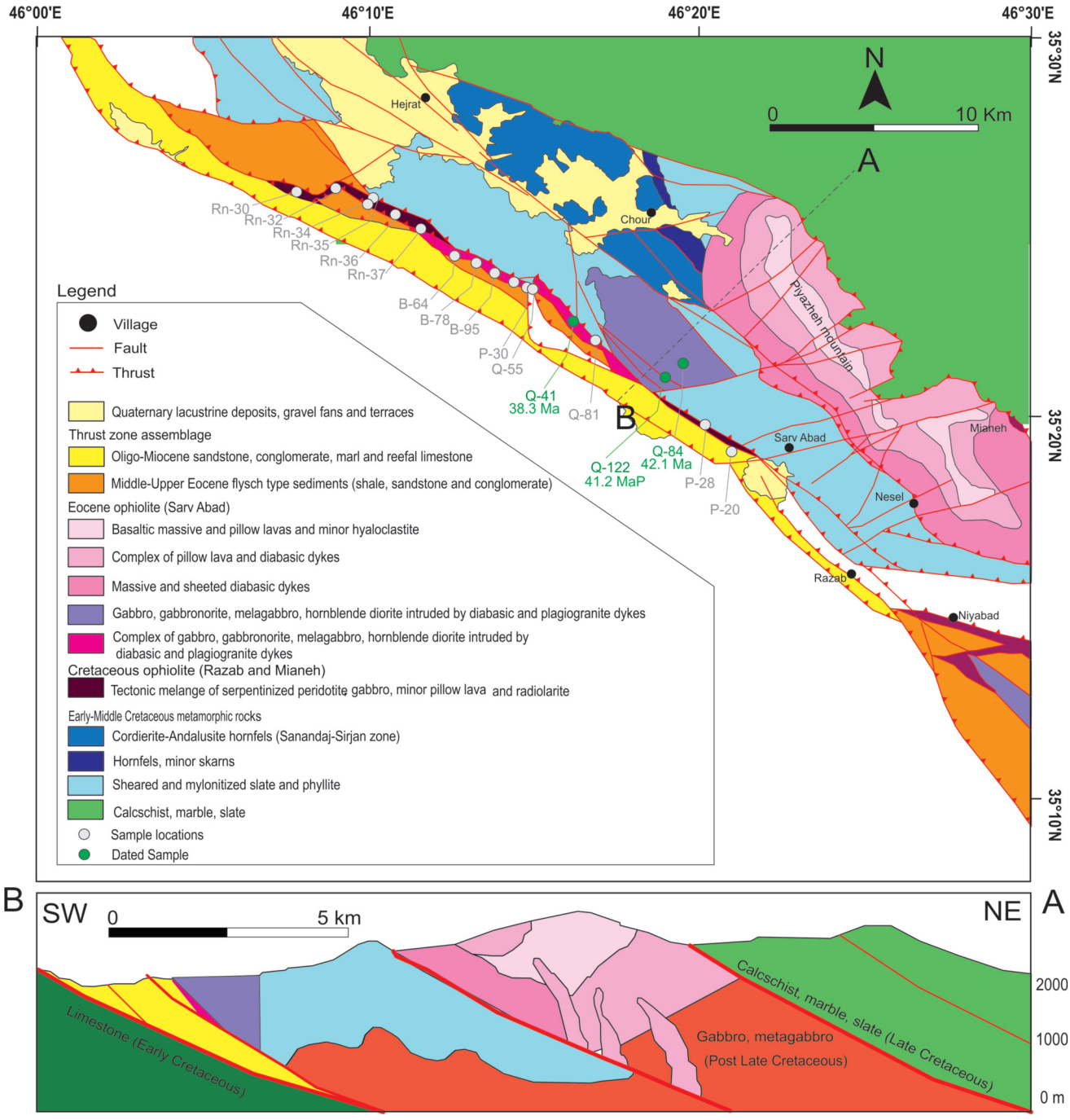

Figure 2. Geological map of the Sarv-Abad ophiolite (Modified after Ghorbani *et al*. 2022).

Sirjan metamorphic rocks consisting of Cretaceous phyllite-slate interlayered with metamorphic limestone; (ii) collisional (thrust) zone units, including a metamorphic complex and related diabasic dikes, basic lava, sandstone, silt, and Eocene flysch, which are located between the Sarv-Abad ophiolites and Bisotun-Avroman subzones (iii) both Razab (Late Cretaceous) and Sarv-Abad (Eocene-Oligocene) ophiolitic complexes, of which the latter includes mantle peridotites, lower crustal gabbros, upper crustal lava, and plagiogranitic and basaltic dikes, and a pre-obduction sedimentary cover (Braud 1987); and (iv) the Bisotun-Avroman zone, including thick and thin layered limestone, limestone-radiolarite, and radiolarite, interlayered by volcanic rock. This oceanic crustal sequence is unconformably overlain by post-obduction Oligocene–Miocene limestone.

In Kurdistan, the Sanandaj–Sirjan zone is a large pre-Permian Arabian–Iranian continental plate that rifted from Arabia during the Late Permian and thus represents a southern Andean-type continental margin of the

Figure 3. (A) Field photo from the Cretaceous Razab ophiolite (Razab village). (B) Serpentinite thrust onto gabbro. (C) Serpentinite. (D) Pillow lava basalt. (E) radiolarite (come from Allahyari *et al*. 2014). Thin section photography from the Cretaceous ophiolite; (F) Pegmatoid gabbro. (G) Microgabbro. (H) Skeletal plagioclase in pillow lava basalt.

Iranian block with abundant calc-alkaline magmatic rocks (Whitechurch *et al*. 2013). This zone comprises a Precambrian-Palaeozoic basement overlain unconformably by Permian–Triassic limestones and Jurassic low-grade metamorphic rocks (phyllites with interbedded metavolcanic rocks). The entire sequence was intruded by Late Jurassic-Late Cretaceous calc-alkaline plutons (Berberian and Berberian, 1981). The metamorphic rocks are unconformably overlain by Barremian–Aptian limestones (Bisotun–Avroman Unit; zone iv) resembling those of the Central Iran block (Stöcklin 1968). The Bisotun-Avroman Unit is composed of thick shallow-water carbonates that range in age from the Late Triassic to Late Cretaceous (Ricou *et al*. 1977; Braud 1987). It is unconformably overlain by shallow marine platform carbonates of the Qom Formation, which were deposited between the Late Oligocene and Early Miocene and include basal conglomerates (Agard *et al*. 2011). The Kurdistan ophiolitic units are structurally characterized by thrust-implicated slices and tectonic contacts. The key structural observations are the Cretaceous Razab and Eocene Sarv-Abad ophiolitic complexes which are separated by a several-hundred-metre-wide zone of intensely sheared rocks belonging to the Sanandaj-Sirjan zone. This zone consists of mylonitic phyllites and schists, with a consistently developed foliation striking NW–SE and dipping steeply to the NE (e.g. Figure 2). The contact between the sheared zone and the ophiolitic units is sharp and tectonic. The Razab ophiolite occurs as a series of ENE-verging thrust sheets. A primary thrust surface places highly serpentinized and mylonitized peridotite over a sequence of gabbro (Figure 3(A,B)). This contact is marked by a ~ 1–2 m thick zone of cataclasite and chlorite-rich fault gouge. The Sarv-Abad complex also displays evidence of syn- and post-magmatic deformation. The serpentinized peridotites exhibit a pervasive foliation, defined by the preferred orientation of serpentine minerals. Isotropic gabbros within the complex are locally mylonitized, showing stretched and recrystallized plagioclase and pyroxene grains (Figure 4(A,E)). These mylonitic zones are cross-cut by networks of brittle, normal faults and are intruded by largely undeformed mafic and felsic dikes (Figure 4(C)), indicating a transition from ductile to brittle deformation. Diabase and plagiogranite dikes within both ophiolitic units

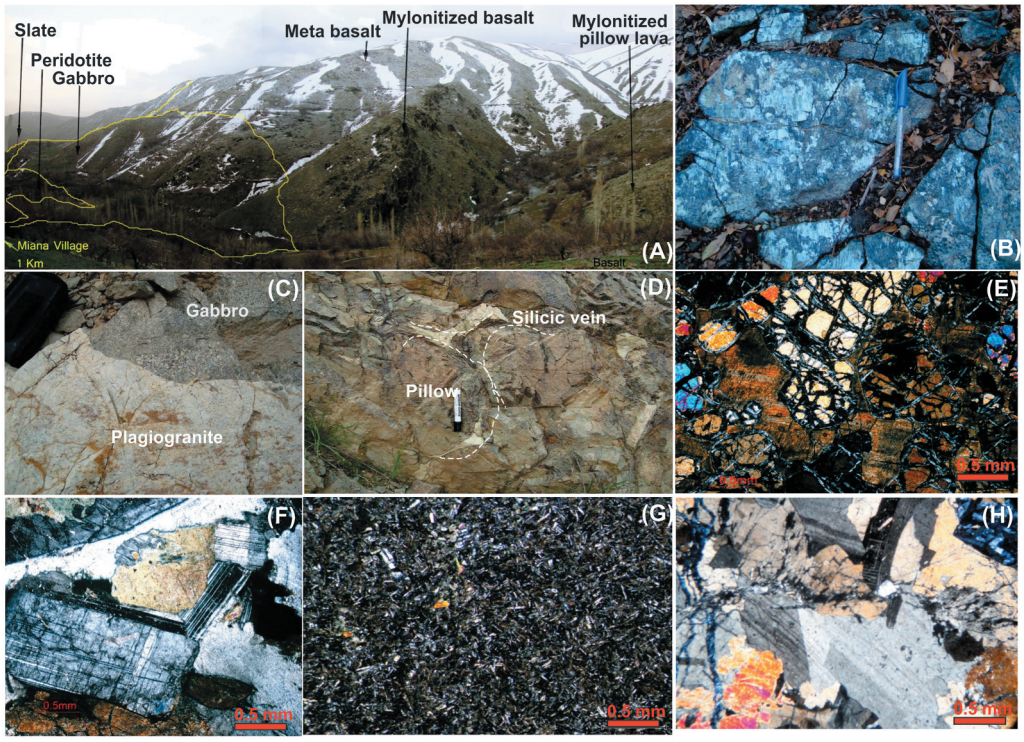

Figure 4. (A) Field photo from Eocene Sarv-Abad ophiolite; (B) peridotite; (C) plagiogranite in isotropic gabbro; (D) pillow lava basalt. Thin section photography from the Eocene ophiolite; (E) dunite (this figure come from Figure 3B of Allahyari *et al*. 2014); (F) pegmatoid gabbro; (G) basalt; and (H) plagiogranite.

commonly exploit pre-existing fracture systems. In the Sarv-Abad complex, these dikes show well-developed chilled margins against the host peridotite and gabbro, and their orientations are often consistent with emplacement along extensional fractures.

2.3. Field observations and petrography

2.3.1. Cretaceous Razab ophiolite

The Cretaceous Razab ophiolite, which occurs as elongated thrusted sheets, consists of highly to completely serpentinized slices of peridotite, cumulate gabbro, pillow lava, diabase, plagiogranite dikes, and radiolarite (Figure 2). These lithologies are separated from the Eocene ophiolites by mylonitic and ultra-mylonitic units of the Sanandaj-Sirjan zone and are tectonically emplaced over (or thrust onto) limestones containing Upper Triassic Megalodons (Braud 1987). The serpentinized peridotite is mylonitized and is in tectonic contact with the gabbro (Figure 3(A–B)). It primarily contains abundant olivine, orthopyroxene, Cr-spinel, and magnetite, with serpentine, chlorite, talc, calcite, and Fe-oxide as secondary phases. Some olivine grains were replaced by serpentine fibres, forming a mesh textures. Subhedral red chromian spinels occur as disseminated grains. Most serpentinites show bastite and mesh textures after orthopyroxene and olivine, respectively, confirming their protoliths are peridotite. All peridotites show deformation textures, including foliations and kink structures. Large coarse- and fine-grained gabbroic intrusions show thrust fault contacts with serpentinized peridotite (Figure 3(B)) and metamorphosed to greenschist and lower amphibolite facies.

Coarse- and fine-grained gabbros show granular (Figure 3(F)), microgranular, or interstitial (Figure 3(G)) textures, and contain plagioclase and pyroxene as major primary mineral, and epidote, albite, chlorite, and calcite as minor secondary phases. The pillow lavas (Figure 3(C)) are covered by Cretaceous radiolarite (Figure 3(D)) and are highly altered and metamorphosed to greenschist facies; however, exposures in Razab village retain original pillow structures (Figure 3(C)). They show porphyritic and interstitial textures consisting of plagioclases and pyroxene as the main minerals in a fine-grained plagioclase, pyroxene, and olivine groundmass. Plagioclase often has a skeletal texture (Figure 3(H))

2.3.2. Eocene Sarv-Abad ophiolite

The Eocene ophiolitic complex located in the Sarv-Abad area is separated from Cretaceous ophiolite occurrences by mylonites belonging to the Sanandaj-Sirjan zone. The Sarv-Abad units consist of several thrust sheets

composed of foliated serpentinized peridotite, gabbro, lava, and intercalated sediments of the Palaeocene to Middle Eocene age (Braud 1987) which are intruded by mafic and felsic (plagiogranite) dikes (Figure 4A). Serpentinized peridotite contains abundant lenticular bodies, lenses, and/or veins of serpentinized dunite (Figure 4B) oriented in the NW-facing direction. All peridotites show deformation textures, such as mylonitization, foliation and kinked structures, stretched and rotated porphyroclasts (~1–3 mm in size), and set in a fine-grained matrix (crystals <0.5 mm in size). They contain olivine (up to 80 vol%), orthopyroxene (up to 15 vol%), augitic clinopyroxene (<5 vol%), and spinel (ca. 1 vol%) (Figure 4E).

Large gabbroic intrusions (Figure 4C) intrude the serpentinized peridotite and are overlain by pillow lava. Foliations within this unit were marked by aligned plagioclase and clinopyroxene/amphibole crystals. The main minerals included euhedral to foliated phenocrysts of plagioclase (~45 vol%) (Figure 4F), pyroxene (~25 vol %), which is mainly augite and diopside, olivine (~5 vol %), amphibole and biotite (~5 vol%), and quartz (<2 vol %). Magnetite, apatite, and ilmenite occur as accessory minerals (<3 vol%). Clinopyroxene contains inclusions of magnetite, amphibole, and biotite and is uralitized and partly replaced by chlorite. Plagiogranites occur as fine- and coarse-grained layers in the gabbroic rocks and show sharp contacts with the surrounding gabbro (Figure 4C). The modal mineralogical compositions of the plagiogranites comprise sodic feldspar (~25 vol%), quartz (35–55 vol%), and plagioclase (40–60 vol%) (Figure 4H), and biotite, hornblende and opaques as accessory minerals. Alteration of plagiogranite formed secondary minerals, such as epidote, kaolinite, chlorite, and sericite. Plagioclase crystals showed polysynthetic zoning. Sodic feldspar crystals likely formed because of the influx of sodic aqueous solutions, thus albitizing primary Ca-rich plagioclase (Ahmadipour and Rostamizadeh 2012).

Lavas form the main crustal exposure of the Sarv-Abad complex. Pillow structures (Figure 4D) occur at the highest stratigraphic level of the adjacent magmatic crustal sequence. The pillows range from 50 cm to 1.5 m in diameter and display vesicular feature. They typically have a centimetre-thick pale green, originally quenched crust and are overlain with fine hyaloclastites and breccias (Figure 4G). Marls and siliceous limestones interbedded with the lavas have Palaeocene–Eocene palaeontological ages (Braud 1987). These igneous rocks are surrounded by limestone and shale, which are attributed to the flysch and turbidity currents of the Cretaceous to Palaeocene age. The pillow lavas preserve primary porphyritic and variably vesiculated textures and are dominated by plagioclase, clinopyroxene, and olivine (in order of abundance), with opaque and fine-grained titanite as accessory minerals. They are locally characterized by secondary minerals of zeolite, calcite, chlorite, albite, and epidote, indicating a low- to medium-grade hydrothermal alteration. The dikes are part of the contiguous magmatic crustal sequence and cut ultramafic sequences, both of which are deformed. The occurrence of plagiogranite dikes is generally limited to the uppermost part of the sequence. They also commonly crosscut ultramafic rocks with well-developed chilled margins. Individual mafic dikes are generally ~0.8–1.5 m wide and can be crystal-rich, containing plagioclase (up to 50%, 0.1–3 cm) and to a lesser extent pyroxene and olivine (~5–10%) phenocrysts and glomerocrysts.

3. Results

3.1. Geochemical compositions

3.1.1. Cretaceous Razab ophiolite

Several lithologies from the Razab ophiolitic sequence, including chromitite, gabbro, and basalt, were analysed for their mineral chemistry (two chromitite samples) and whole-rock major and trace element (six samples) contents. Results from chromitite samples show that spinel has low Al_2O_3 (7.4–11.5 wt%) and TiO_2 (0.08–0.22 wt%), high FeO^{tot} (19.3–23.0 wt%) and Cr_2O_3 (49.7–57.1 wt%) contents. Spinel MnO contents are consistently low (-0.10–0.32 wt%) (Suppl. Table S1a). These low values reflect Mn partitioning into melts during high-degree melting, consistent with the formation of a depleted mantle residue (Barnes *et al*. 2014). This spinel has Mg# = 0.52–0.72 (mean value = 0.57) and Cr# = 0.77–0.82 (mean value = 0.79) (Supplementary Appendix; Suppl. Table S1a).

Based on their geochemical features, the lavas (four samples) investigated in this study were subdivided into two main groups (Suppl. Table S2a): (i) subalkaline basalt with high SiO_2 (47.9–54.2 wt%) and MgO (6.6–9.9 wt%), low Fe_2O_3 (8.5–9.6 wt%), CaO (8.6–9.6 wt%), and TiO_2 (1.0–1.2 wt%), and moderate Al_2O_3 (-13.4–14.6 wt%) and (ii) alkaline basalt with lower SiO_2 (45.7–46.6 wt%) and MgO (3.8–4.0 wt%) and higher Fe_2O_3 (11.3–12.6 wt%) and CaO (10.5–12.3 wt%), and TiO_2 (3.5–4.0 wt%), and the same Al_2O_3 (13.4–14.6 wt %) contents. On total Nb/Y vs. Zr/Ti (LeMaitre *et al*. 2002) and Co vs. Th (after Pearce 1996) diagrams, all lavas fall in the 'basalt' and 'alkaline basalt' fields and have island arc tholeiitic (IAT)/back-arc and calc-alkaline affinities, respectively (Figure 5A–B). Both basaltic lavas are also characterized by Ti/V ratios 20 to 30 and 72 to 81, in agreement with N-MORB and

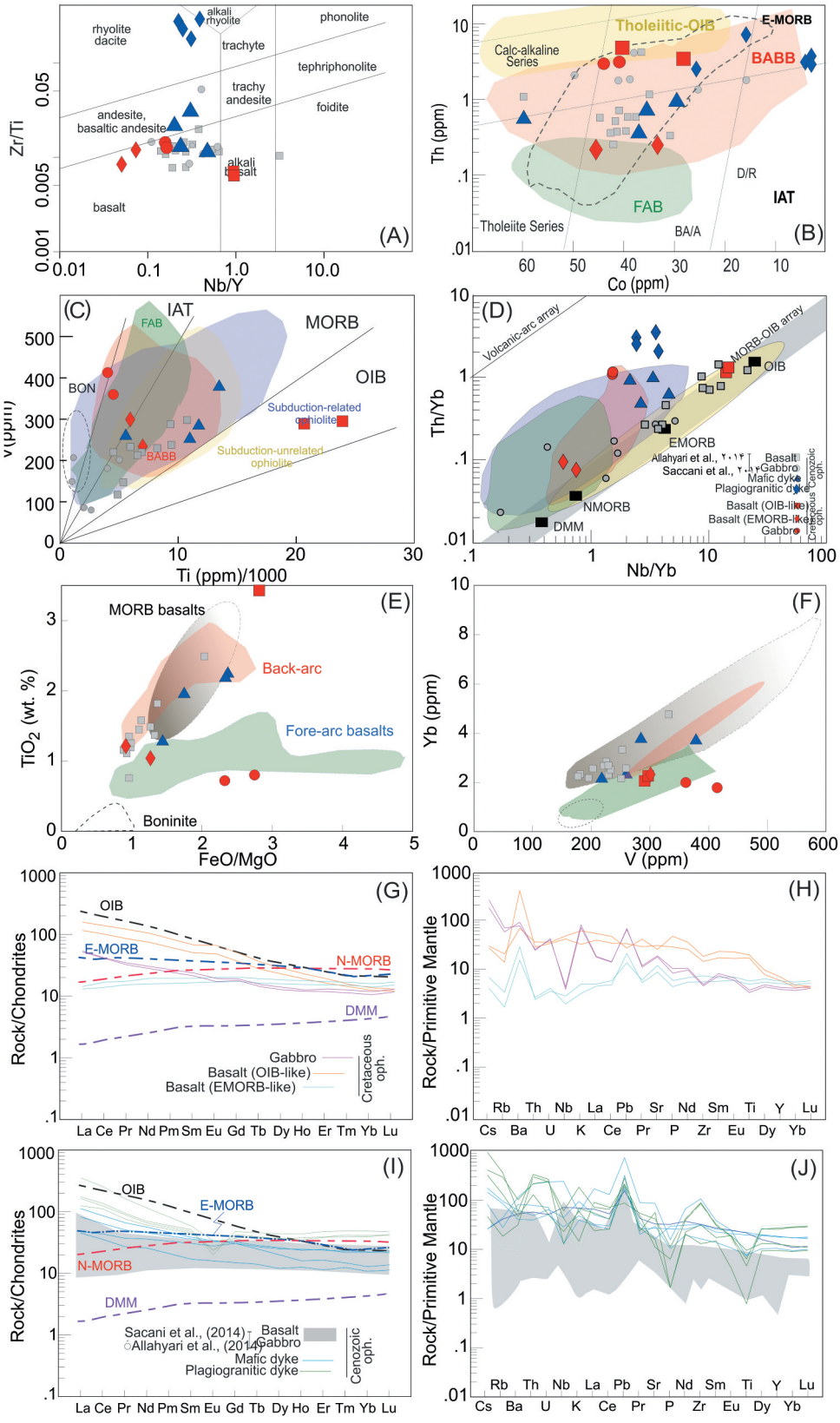

Figure 5. Whole-rock geochemistry of mafic rocks and felsic dike from the Razab and Sarv-Abad ophiolite complex. (A) Nb/Y vs. Zr/Ti plot (after Pearce (1996)); (B) Th vs. Co diagram (Hastie *et al*. 2007). Rock type: B, basalt; BA/A, basaltic andesites/andesites; CA, calc-alkaline series; D/R, dacite/rhyolite; H–K, high-K series; IAT, island arc tholeiitic. Petrological group and references: BABB, back-arc basalts (Pearce and Stern 2006); FAB, forearc basalts (Reagan *et al*. 2010); tholeiite-OIB, ocean island basalts (Buchs *et al*. 2011); E-MORB, enriched mid-ocean ridge basalts (after O'Neill and Jenner 2012); 85% probability contour of island arc tholeiite composition (after Hastie *et al*. 2007); (C–D) V (ppm) vs. Ti/1000 (ppm) (after Shervais 1982, Reagan *et al*. 2010; Rossetti *et al*. 2017). (C, D) Nb/Yb vs. Th/Yb diagram (after Pearce 2008; Rossetti *et al*. 2017). Petrological groups and references as in Figure 5. Fields of 'subduction-related

OIB-like mafic rocks, respectively (Figure 5(C–D)). Basalts with Ti/V ratios in the range 20–30 (average = 25) mainly show a MORB and/or fore-arc affinity in TiO_2 vs. FeO/MgO and Yb vs. V diagrams (Figure 5E–F) (Lázaro *et al*. 2016). Their chondrite-normalized LREE contents show a slight depletion and plot near the N-MORB field, with $(La/Yb)_N$ and $(Dy/Yb)_N$ having mean values of 0.86 and 1.1, respectively (Figure 5G). In the PM-normalized multi-element diagrams (Sun and McDonough 1989), the Razab basalts have slightly negative Nb and Ti anomalies (Figure 6(H)). In contrast, alkaline basalts show high Ti/V ratios of 71–81, which are similar to oceanic island basalt (OIB) Ti/V ratios of 50–100 (Shervais 1982) (Figure 5(C)). They plot within the mantle-OIB array close to OIB field in the Th/Yb vs. Nb/Yb diagram (Figure 5(D)) and show fore-arc affinity in Yb vs. V diagram (Figure 5F). Their chondrite-normalized patterns display enrichment in LREE and plot near the OIB field, with $(La/Yb)_N$ and $(Dy/Yb)_N$ mean values of 9.62 and 1.9, respectively (Figure 5(G)). They were enriched and lacked Nb- and Ti-negative anomalies (Figure 5(H)).

The two gabbro samples from Razab have SiO_2 = 50.1–50.3 wt%, Al_2O_3 = 15.5–15.9 wt%, CaO = 5.8–6.6 wt %, FeO = 12.3–13.3 wt%, and TiO_2 = 0.7–0.8 wt%. The sample plot within the 'basalt' and calc-alkaline fields on the Nb/Y vs. Zr/Ti diagram (Winchester and Floyd 1977). This diagram, although designed for volcanic rocks, is routinely applied to coarser grained intrusive rocks like gabbro to infer their tectono-magmatic affinity (Figure 5(A–B)). The gabbros showed Ti/V ratios in the range of 10–13 (average = 11), which resemble island-arc basalt signatures (Shervais 1982). They also show affinity to mafic magma with signatures of BABB/fore-arc, as shown in the V vs. Ti/1000 and Th/Yb vs. Nb/Yb diagrams (Figure 5(C–D)). On diagrams used to discriminate between forearc and BABB basins (TiO_2 vs. FeO/MgO and Yb vs. V), the gabbros predominantly plot within the forearc field. However, two samples with high Al_2O_3 (>18 wt%) deviate from this trend, likely due to plagioclase accumulation. In the chondrite-normalized REE diagram (Sun and McDonough 1989), the gabbros display $(La/Yb)_N$ and $(Dy/Yb)_N$ mean values of 4.4 and 1.1, respectively. The Eu anomaly was slightly negative (average = 0.9). In PM-normalized trace element diagram (Sun and McDonough 1989) (Figure 5I–J) gabbros show profiles similar to those of PM. They are characterized by the depletion of LILEs (such as Th) and HFSEs (such as Ti, Zr, and Hf) with respect to clear positive anomalies of Nd and Eu (REEs).

3.1.2. Eocene Sarv-Abad ophiolite

Units of the Sarv-Abad ophiolitic sequences, including peridotite, gabbros, and basalts (Allahyari *et al*. 2014; Saccani *et al*. 2014; Supp. Table S2b) and diabase and plagiogranite dikes (this study; Suppl. Table S2c) were evaluated for mineral chemistry and whole-rock major and trace elements.

The spinel in the Sarv-Abad peridotite shows variable Al_2O_3 (14.5–21.5 wt%) and FeO^{tot} (22.5–28.5 wt%) with high Cr_2O_3 (32.4–44.9 wt%) contents, but low MnO (<1.1 wt%) and TiO_2 (0.06–0.32 wt%) values (Allahyari *et al*. 2014). The spinel showed Mg# of 0.5–0.7 (mean value = 0.5) and Cr# of 0.5–0.7 (mean value = 0.6) (Supp. Table S1b; Allahyari *et al*. 2014). The spinel in the Sarv-Abad chromitite has lower Al_2O_3 (10.9–11.4 wt%), and higher Cr_2O_3 (56.3–57.1 wt%) contents than those of the peridotite. This spinel is characterized by narrow ranges in Mg# (0.49–0.54; average = 0.52) and Cr# (0.77–0.78; average = 0.77) (Supp. Table S1b; Allahyari *et al*. 2014), falling within the ranges of abyssal and forearc peridotites. Olivine from the Sarv-Abad peridotite has a similar composition, having low MnO (0.1–0.2 wt%) and Cr_2O_3 (<0.1 wt%) contents. Their Fo = 89–91 mol% and NiO = up to 0.4 wt% (Supp. Table S1b; Allahyari *et al*. 2014) resembles residual mantle olivine (e.g. Arai 1994; Khedr *et al*. 2013, 2014) that formed at the intersection of abyssal and forearc peridotites (Pagé *et al*. 2008).

The Sarv-Abad peridotite samples show loss of ignition (LOI) values in the range 7.6–12.3 wt%, signifying moderate-to-high degrees of serpentinization (Supp. Table S2b; Allahyari *et al*. 2014). They had low SiO_2 (37.1–40.5 wt%), Al_2O_3 (0.7–1.7 wt%), CaO (up to 1 wt%), and TiO_2 (0.02–0.13 wt%) contents. The CaO/Al_2O_3 (0.12–0.5) and Mg# (0.88–0.91) ratios, and Cr (1313–2686 ppm) and Ni (2005–2469 ppm) contents are close to the PM values (CaO/Al_2O_3 = 0.8, Mg# = 0.88, Cr = 3240 ppm; Hart and Zindler 1986; McDonough and Sun 1995; Workman and Hart 2005), showing a peridotite with refractory character (Al_2O_3/SiO_2 < 0.05 and MgO/SiO_2 = 0.98–1.1). In a chondrite-normalized diagram (Sun and McDonough 1989) (Figure 6(A)), the Sarv-Abad peridotites show LREE

ophiolite' and 'subduction unrelated ophiolite' are after Dilek and Furnes (2011, 2014)). Field of boninite (BON) in is after Dilek and Furnes (2011). Average lower crust (LC), average upper crust (UC), total continental crust, average assimilation-fractionation trends (dashed arrows), and trend of crustal recycling (dashed line) are from Pearce (2008) and are reported in diagram (D) for comparison; (E) Chemical variation for the TiO_2 vs. FeOt/MgO and (F) V vs. Yb diagrams (Lázaro *et al*., 2016). (G) chondrite-normalized rare earth element (REE) diagrams (Sun and McDonough 1989) and (H) primitive mantle-normalized multi-element diagrams (Sun and McDonough 1989) for the Sarv-Abad crustal sequences, respectively.

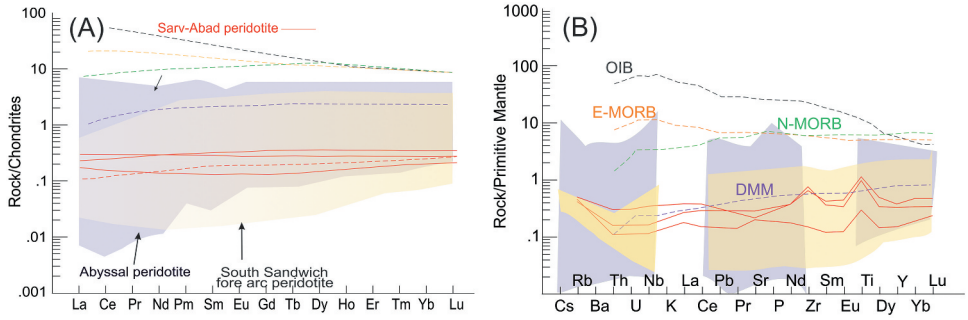

Figure 6. (A) Chondrite-normalized rare earth element (REE) and (B) primitive mantle-normalized diagrams (Sun and McDonough 1989) for Sarv-Abad peridotites. Data for OIB, N-MORB, and E-MORB are after Sun and McDonough (1989), abyssal peridotites are after Niu and Batiza (1997) and Lian *et al*. (2019), and South Sandwich forearc peridotites are after Pearce *et al*. (2000). This figure has been modified from Figure 7 of Sepidbar *et al*. (2020).

to HREE sub-chondritic flat profiles, with $(La/Yb)_N$ and $(Dy/Yb)_N$ values of 0.5–1.13 and 0.007–1.03, respectively (Figure 6(A)). In a PM-normalized multi-element diagram (Sun and McDonough 1989) (Figure 6(B)), the peridotites show slightly depleted profiles with a minor enrichment of HFSEs (e.g. Zr and Ti). The Sarv-Abad peridotites are similar to abyssal peridotites (Figure 6) and have compositional similarity to those from the South-Sandwich arc-basin system (SSABS) (Pearce *et al*. 2000).

The major element composition of the whole-rock lava is basaltic (Figure 5A), with variable MgO = 6.6–-10.9 wt% (Mg# = 0.54–074) contents and very little evidence of hydrous alteration (L.O.I. = 1.1–3.0 wt%) (Supp. Table S2b; Allahyari *et al*. 2014; Saccani *et al*. 2014). They are characterized by SiO_2 = 45.2–51.5 wt%, with moderate Al_2O_3 (13.5–15.6 wt%), FeO (5.1–10.3 wt%), CaO (6.7-–12.7 wt%), and TiO_2 (0.7–1.8 wt%). On Nb/Y vs. Zr/Ti (Winchester and Floyd 1977) and Co vs. Th (after Pearce 1996) diagrams, all basalts fall in the 'basalt' field with calc-alkaline affinity, except for one sample that shows a tholeiitic island arc signature (Figure 5(B–C)). They show moderate Cr (131–769 ppm), Ni (27–270 ppm), and V (116–297 ppm). The basalts contain TiO_2 = 0.7–1.8 wt% wt% and have Ti/V values of 25–45 (average = 35), which are E-MORB-like signatures (Shervais 1982). They also showed affinity to mafic lava with signatures between MORB in the Ti vs. V and Th/Yb vs. Nb/Yb (Figure 5(C–D)) diagrams. These diagrams indicate that most of the studied samples fall within or very close to the field of the back-arc and MORB basalts (Figure 5(C–E)).

Magmatic major element fractionation trends can be disrupted by crystal accumulation or hydrothermal alteration. The following geochemical characterization thus focuses on immobile or little-mobile trace elements (TiO_2, Zr, Y, Nb, V, Yb, and REEs) that largely remain unaffected by alteration and low-grade metamorphism (e.g. Seyfried *et al*. 1988; Gillis and Thompson 1993; Hofmann and Wilson 2007; Furnes *et al*. 2012). Following the definitions from Gale *et al*. (2013), most lavas have MORB-like to back-arc-like TiO_2, Zr, Y, and Nb contents (Nb/Y <0.8, 'low-Nb') and variable REE compositions that range from D-MORB (La_N/Sm_N <0.8; McDonough and Sun 1995) to E-MORB (La_N/Sm_N >1). They also show affinity to mafic lava with signatures between the MORB and back-arc in the V vs. Yb (Figure 5F) diagram. Most compositions overlap (La_N/Yb_N = 0.82–1.9), although one mafic sample is slightly more enriched (La_N/Yb_N = 7.06), indicating two geochemical types: LREE-depleted and LREE-enriched (Figure 5(I)). Those with slightly depleted LREE lie near the N-MORB field, whereas slightly enriched LREE samples plot near the E-MORB field. The rocks with slightly depleted LREE contents have $(La/Yb)_N$ and $(Dy/Yb)_N$ mean values of 0.8–1.9 and 1.1–1.2, respectively, with a lack of Eu anomaly (average = 1.0). In contrast, LREE-enriched samples had average $(La/Yb)_N$ and $(Dy/Yb)_N$ values of 7.06 and 1.2, respectively (Figure 5J). In PM-normalized multi-element diagrams (Sun and McDonough 1989), both types of Sarv-Abad basalts show enriched patterns, without Nb and Ti negative anomalies (Figure 5H). They show affinities for normal and enriched-type mid-ocean ridge basalts (N-MORB and E-MORB, respectively) (Sun and McDonough 1989).

The gabbro samples have SiO_2 = 47.1–50.7 wt%, Al_2O_3 = 14.6–19.3 wt%, CaO = 10.6–13.5 wt%, FeO = 3.6–7.5 wt%, TiO_2 = 0.2–0.8 wt%, Cr = 99–705 ppm, Ni = 83–463 ppm, and V = 35–205 ppm (Supp. Table 2b; Allahyari *et al*. 2014; Saccani *et al*. 2014). All fall in the field of 'basalt and basaltic andesite', which lie within the trachyandesite and calc-alkaline series on the Nb/Y vs. Zr/Ti diagram (Winchester and Floyd 1977) and Co vs. Th (after Pearce 1996) (Figure 5(A–B)). The gabbros contain TiO_2 = 0.17–0.84 wt% and have Ti/V values of 16–35

(average = 23), which are E-MORB-like signatures (Shervais 1982) (Figure 5(C)). They also showed affinity to mafic lava with signatures of MORB in the Ti vs. V and Th/Yb vs. Nb/Yb (Figure 5(C–D)) diagrams (Pearce 2008). These diagrams indicate that most of the studied samples fall within or very close to the field of the back-arc and MORB basalts (Figure 5(C–E)). They show heterogeneous LILE (e.g. Sr: 81–237 ppm) and HFSE (e.g. Nb: 0.1–5.4 ppm, Y: 5–11 ppm, and Zr: 2–54 ppm) contents. In addition, some gabbros have TiO_2, Zr, Y, and Nb contents (Nb/Y: <0.8; "low-Nb) and REE compositions ($La_N/Sm_N < 1$; $La_N/Yb_N = 0.8–1.2$; McDonough and Sun 1995) resembling D-MORB (definitions from Gale *et al*. 2013). In contrast, some have more enriched features with Y and Nb contents (Nb/Y = 1.6–6.93; 'high-Nb') and REE compositions resembling E-MORB ($La_N/Sm_N > 1$; $La_N/Yb_N = 1.7$, with lack an Eu anomaly (mean value of ~1.0; McDonough and Sun 1995). The chondrite-normalized REE pattern is rather flat in the MREE–HREE plots (at approximate 10–13 × C1) and is relatively LREE enriched ($La_N/Sm_N > 1$).

The major and trace element whole-rock compositions of the diabase and plagiogranite dikes are reported in Suppl. Table S2c. The mafic dikes have SiO_2 = 41.7–53.8 wt%, Al_2O_3 = 14.0–18.3 wt%, FeO = 9.3–13.2 wt%, CaO = 4.6–12.4 wt%, and TiO_2 = 0.6–2.3 wt% and show variable LOI contents (2.4–8.6 wt%; Table 2). All mafic dikes lie in the field of 'basalt and basaltic andesite', which lie within the tholeiitic series on the Nb/Y vs. Zr/Ti diagram (Winchester and Floyd 1977) and Co vs. Th (after Pearce 1996) (Figure 5(A–B)). The samples show TiO_2 = 1.22–2.25 wt% and Ti/V ratios of 28–41 (average = 35) mainly show E-MORB-like signature (Shervais 1982). They also show affinity to mafic magma with signatures of BABB, as shown in the V vs. Ti/1000 and Th/Yb vs. Nb/Yb diagrams (Figure 5(C–D)). The TiO_2 vs. FeO/MgO (Figure 5(E)) and Yb vs. V (Figure 5(F)) diagrams are also used to discriminate between forearc and BABB basins; In such diagrams, mafic dike show geochemical affinity to back-arc basin basalts. All the diabase dikes have MORB-like Y and Nb contents (Nb/Y < 0.8, 'low-Nb') but have REE compositions comparable to those of E-MORB ($La_N/Sm_N > 1.5$; Suppl. Table S2c). They are slightly more enriched (La_N/Yb_N = 1.9–8.2, average = 4.4, $n = 4$) than the lava (La_N/Yb_N = 0.85–1.9, with one analysis of 7.1), with average 1.4, $n = 5$.

The Sarv-Abad plagiogranite dikes have higher SiO_2 contents (62.8–72.1 wt%) than the diabase dikes (Suppl. Table S2c) and are enriched in Na_2O (5.4–9.6 wt%) and depleted in K_2O (0.1–0.2 wt%) (Suppl. Table S2c), which are characteristic of plagiogranites (Coleman and Peterman 1975) worldwide. The high Na_2O contents are consistent with secondary albitization. The total REE content of the plagiogranite varies from 90 to 220 ppm, which are generally higher than that of diabase dikes (62.0–117 ppm). They are relatively enriched in LREE (Figure 5(I)), with $(La/Yb)_N$ ratios of 2.2–8.3 and negative Eu anomalies (0.3–0.6; except for one samples with positive value of 1.17) (Figure 5(I)). Most plagiogranites are depleted in HFSE (Nb, Ti, and P) and enriched in LILE (Rb and K) (Figure 5(J)).

3.2. Geochronology

3.2.1. Cretaceous (Razab) ophiolite

Samples from Razab, collected from radiolarian cherts, contain radiolarians that are strongly recrystallized and abundant sponge spicules. These spicules are Mesozoic and probably Jurassic–Cretaceous in age (not Triassic), although a precise stratigraphic age cannot be obtained from them as sponges typically show very slow evolutionary changes (Supplementary Appendix S1; Supplementary Figure S1).

3.2.2. Cenozoic (Sarv-Abad) ophiolites

U–Pb dating was performed on zircons from one gabbro and two plagiogranite dikes from the Sarv-Abad ophiolite (Suppl. Table S4). Zircons from gabbro sample Q-41 were euhedral prismatic crystals of 100–250 µm in length with aspect ratios of 2:1–3:1. These are typical magmatic zircons with clear oscillatory zoning and high Th/U ratios (0.99–1.07). The $^{206}Pb/^{238}U$ apparent ages of three points range from 37.4 Ma to 38.98 Ma, with a weighted average of 38.4 ± 1.3 Ma (2σ; MSWD = 0.2) (Figure 7A). Zircons from two plagiogranitic dikes (Q-122 and Q-81) were euhedral prismatic crystals of 100–300 µm in length with aspect ratios of 1:1–3:1. The zircons are magmatic with clear oscillatory zoning and high Th/U ratios (1.0–1.3 and 0.5–1.4, respectively). The $^{206}Pb/^{238}U$ apparent ages of six analyses from Q-81 range from 38.1 Ma to 50.69 Ma, with a weighted average value of 41.2 ± 1.0 Ma (2σ; MSWD = 0.02) and three analyses from Q-122 range from 37.8 Ma to 43.9 Ma, with a weighted average value of 42.1 ± 1.1 Ma (2σ; MSWD = 0.001) (Figure 7B–C). While the small number of analyses warrants caution, this age is interpreted as the best current estimate for the crystallization of this gabbroic unit. In addition, these ages are overlapping within their overestimated analytical uncertainties and define a preliminary crystallization age for this unit in the latest Eocene.

4. Discussion

The Kurdistan ophiolite complexes comprise the Eocene Sarv-Abad and Cretaceous Razab ophiolites. Both sequences contain mantle and crustal components,

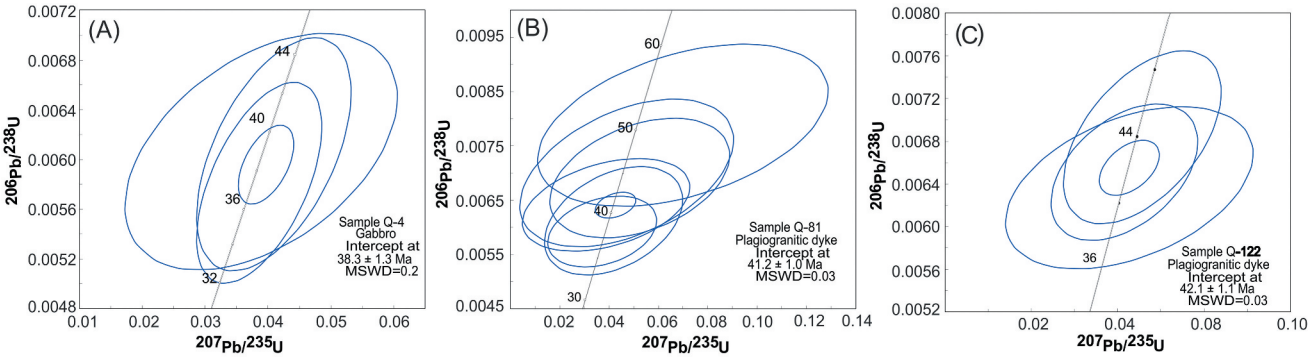

Figure 7. Zircon U–Pb Concordia diagrams show the $^{206}Pb/^{238}U$ ages of the analysed zircons with 2 sigma errors for samples Q-41 (A), Q-81 (B), and Q-122 (C).

including peridotites, gabbros, and diabase-sheeted dikes and extrusive sequences, including pillow lava, and mafic and felsic (plagiogranite) dikes. The geochemical and geochronological results obtained in this work provide a context for understanding the chemical and temporal evolution of the Kurdistan ophiolite complex. Our data reveal that the Eocene Sarv-Abad crust was constructed by contemporaneous magmatism producing both D-MORB and E-MORB signatures. Specifically, the ~41–38-Ma gabbros and cross-cutting mafic dikes encompass the full range from D-MORB to E-MORB compositions, indicating a heterogeneous mantle source was melting simultaneously during this period. This challenges models that attribute such geochemical diversity solely to temporal variations in parental melt components (e.g. Batiza and Niu 1992) and instead highlight the importance of spatial mantle heterogeneity. A revised geochronological and tectonic model for Kurdistan ophiolites has also been proposed.

4.1. Chemical evolution of Kurdistan ophiolites

4.1.1. Petrogenesis of Kurdistan ultramafic melts

The whole-rock compositions of peridotites from the Cretaceous Razab and Eocene Sarv-Abad ophiolite complexes, along with their mineral assemblages (Spl + Ol + Px) and chemistry, record the nature and evolution of the Kurdistan ultramafic rocks. The Cr-spinel from the Razab chromitite has high Cr# (0.76–0.82, average = 0.79) and Mg# (0.53–0.72, average = 0.57), which resemble those found in forearc environments (Mg# = 0.45–-0.65; Cr# = 0.40–0.80; Parkinson and Pearce 1998), and shows some similarity with those that form in SSZ settings (e.g. Ishii *et al*. 1992; Khedr and Arai 2017). This aligns with field evidence of mylonitization (Figure 3(A–B)) and supports the subduction–initiation process. When combined with the occurrence of forearc basalt (FAB)-like lavas in the sequence, these high-Cr# spinels are consistent with a forearc setting and provide supporting evidence for a subduction initiation environment. This interpretation is further strengthened by the similarity of our peridotites' refractory compositions characterized by high-Cr# spinel and depleted major elements to those documented in the mantle sections of the Kurdistan ophiolites (Nouri *et al*. 2018), the Makran (Sepidbar *et al*. 2020), and the South Sandwich arc-basin system (Pearce *et al*. 2000).

The Cr-spinel in the Sarv-Abad peridotites has a high Cr# (0.58–0.69, average = 0.64) and Mg# (0.48–0.65, average = 0.57). This composition is indicative of a depleted mantle source that underwent melting in a supra-subduction zone setting, rather than in a mid-ocean ridge or simple extensional basin. Based on Mg#, Cr#, and Al–Cr–Fe^{3+} values, spinel analyses show affinities to forearc (Mg# = 0.45–0.65; Cr# = 0.40–0.80; Parkinson and Pearce 1998) and abyssal peridotites (Mg# = 0.45–0.85; Cr# = 0.10–0.60; Warren, 2016). The Fo (88–91 mol%) and NiO (0.22–0.56 wt%) contents of olivine from the Sarv-Abad peridotites resembles residual mantle olivine (Fo = 89–92 mol%; NiO = 0.20–0.55 wt%; after Pagé *et al*. 2008). The Cr# of spinel and Fo content of olivine in Sarv-Abad peridotites corresponds with the olivine – spinel mantle array ($Fo_{olivine}$ = 88–94; OSMA; Arai 1994), abyssal peridotites ($Cr\#_{Spinel}$ = 0.10–0.60; $Fo_{olivine}$ = 0.90–0.92; after Arai 1994), and SSZ peridotites ($Cr\#_{Spinel}$ = 0.30–-0.85; $Fo_{olivine}$ = 0.90–0.93; Pearce *et al*. 2000). The study samples are therefore similar to peridotites from the Izu–Bonin–Mariana fore-arc peridotites (Pearce *et al*. 2000), and we interpret that the Sarv-Abad peridotites are moderately depleted and originated in an SSZ setting. The relationships between spinel Cr# and olivine Fo content (not shown) show that the Sarv-Abad peridotite represents a mantle residuum that formed after 20–30 vol%, melt extraction from a pristine fertile MORB mantle (FMM; e.g. Khedr and Arai 2017). The geochemical characteristics of the Sarv-Abad peridotite, such as MgO

(38.1–42.8 wt%), CaO (0.22–02.56 wt%), and Al_2O_3 (0.75-–1.86 wt%) contents (Supp. Table S2b) are typical of depleted mantle (MgO = 38.73 wt%; CaO = 0.7–2.8 wt %, and Al_2O_3 = 0.7–3.0 wt%; Pearce *et al*. 1992), signifying that these ultramafic units experienced partial melting and extraction of melts (Lian *et al*. 2019). The elevated MgO/SiO_2 ratios (average = 1.04) and depleted Al_2O_3/SiO_2 ratios (average = 0.03) (Supp. Table S2b) in the Sarv-Abad peridotite samples compared to PM (MgO/SiO_2 = 0.8; Al_2O_3/SiO_2 = 0.1; after McDonough and Sun 1995; Workman and Hart 2005) and depleted mantle MORB (DMM) (MgO/SiO_2 = 0.84; Al_2O_3/SiO_2 = 0.10; after McDonough and Sun 1995) also specify that the Sarv-Abad peridotites are mantle residues that form following moderate-to-high degrees of melt extraction (Barnes *et al*. 2014; Lian *et al*. 2019).

4.1.2. Petrogenesis of Kurdistan mafic melts

The Razab mafic suite contains gabbro cross-cut by diabase dikes and overlain by pillow lavas. The minimum Cretaceous age for basaltic lavas eruption and emplacement can be inferred from the age of the radiolarite that covers the pillow lavas. The primary contact between the gabbros and upper pillow lava and the presence of cross-cutting diabase dikes require a relatively older age for the gabbros, which must have solidified prior to basaltic eruption and diabase emplacement. The geochemical bimodality observed in the Razab basalts, with one group (Rn-34 and Rn-35; Ti/V = 20–30) showing IAT/forearc affinities and the other (Rn-30 and Rn-32; Ti/V = ~70–80, Nb/Y > 0.7) showing OIB-like signatures, is a diagnostic feature of subduction initiation zones. This is consistent with a model where early decompression melting of upwelling, uncontaminated asthenosphere (yielding the OIB-like basalts) is rapidly succeeded by flux melting of the metasomatized mantle wedge (yielding the IAT-like basalts) as the slab sinks and hydrous fluids are released. The isotropic gabbros record enriched REE and trace-element patterns comparable to E-MORB and high-Ti N-MORB melts. In the context of a maturing proto-forearc, this enrichment is unlikely to represent the initial mantle source. Instead, it is more consistent with the percolation and trapping of late-stage, more enriched melts within the lower crust, potentially reflecting the waning stages of magmatism or infiltration of melts from a more fertile mantle domain as the system evolved from initial spreading towards early arc volcanism (Saccani *et al*. 2018).

The consistent Nb, Th, and Ti depletion in gabbro and some DMM and the N-MOR mafic rocks again supports magma genesis in an SSZ environment (e.g. Khedr and Arai 2017; Rossetti *et al*. 2017). The Ti/V ratios can be used as a reliable geochemical proxy for discriminating between distinct tectonic settings. Specifically, arc-related magmas (including SSZ and IAT) typically exhibit Ti/V ratios of <20, whereas mid-ocean ridge basalts (MORB) and ocean island basalts (OIB) are characterized by Ti/V ratios of 20–50 and >50, respectively (Shervais 1982). While basalts have an OIB-like (~72–81) and N-MORB (~20) characters, gabbros from Razab have Ti/V ratios of ~10–30. These values are transitional and are most consistent with a back-arc basin (BABB) affinity, which is characteristic of the evolving magmatic systems in Early Cretaceous arc-basin settings. Additionally, Nb/Y ratios are widely employed to assess mantle enrichment processes (Pearce 2008). In this scheme, depleted mantle sources (N-MORB) yield Nb/Y values of <0.2, transitional mantle sources (E-MORB) range between 0.2 and 0.7, and enriched mantle signatures (OIB) display values >0.7. The Razab basalts exhibit distinct Nb/Y ratios, with N-MORB samples showing low values (0.06) and OIB samples displaying higher ratios (1.09), consistent with the MORB-OIB array. In contrast, the E-MORB and calc-alkaline arc-related gabbros have lower Nb/Y ratios (0.08–0.16) and plot above the MORB-OIB array towards the composition of the subducted sediments and/or assimilation of lower continental crust components (Supplementary Figure S2A; after Pearce 2008). In summary, the Razab mafic magmatic rocks (especially N-MORB basalts and gabbros) are characterized by an IAT and calc-alkaline signature (Figure 5B; Hastie *et al*. 2007), respectively, a subduction-related ophiolite (Th/Yb vs. Nb/Yb diagram in Supplementary Figure S2A; after Dilek and Furnes 2011), and a main forearc affinity (FAB in Th vs. Gd/Lu diagram; modified after Deschamps *et al*. 2013) (Supplementary Figure S2B). The Sarv-Abad mafic suite also contains basalt, gabbro, diabase, and felsic dikes. Our data also show that the different gabbro, lava, and dike groups on Sarv-Abad have variable ranges in trace element concentrations that overlap with the MORB array (from N-MORB to E-MORB) and extend to more enriched LREE compositions in the younger mafic dikes (Figure 5). The Ti/V ratios of basaltic diabase have an OIB-like (~130) and N-MORB (~22–41) characters, which can be also deduced as distinctive evolution of Early Cenozoic basin systems. In addition, their Nb/Y ratios are in agreement with transitional mantle sources (E-MORB) range between 0.2 and 0.7, and plot above the MORB-OIB array

The minor variations in MgO, Cr, and Ni contents between lava and gabbro, along with the restricted thickness of the gabbroic lower crust, argue against a secondary role for magmatic fractionation in the formation of trace element variations. While low degrees of partial melting can generate trace element enrichment, the coexistence of D-MORB and E-MORB signatures in

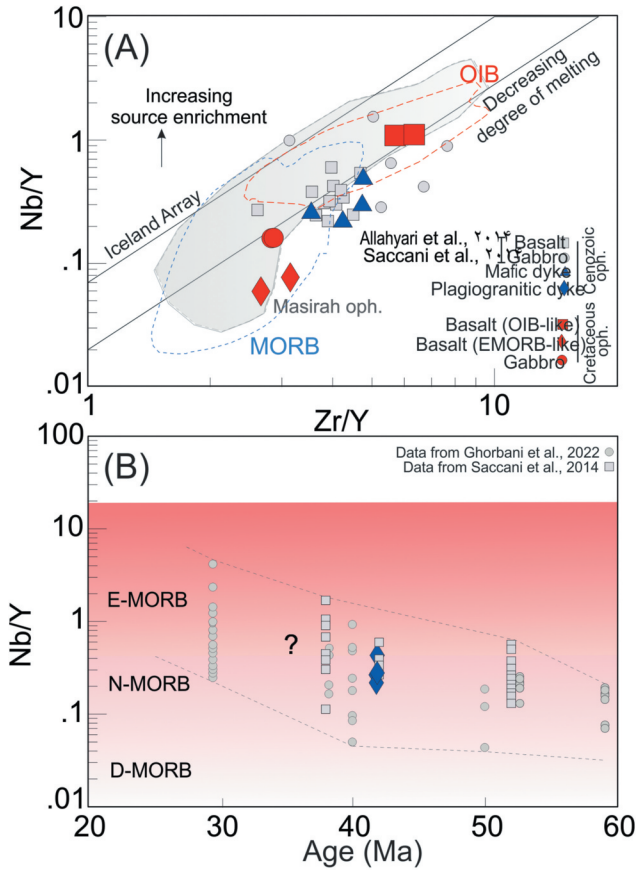

Figure 8. (A) Nb/Y vs. Zr/Y trace element diagram (excluding data with MgO < 5 wt%) after Fitton *et al*. (1997), showing the effects of source enrichment vs. degree of melting. (B) The range of Nb/Y vs. ages in the Sarv-Abad dikes and lava-gabbro. Ranges for present-day N-MORB (all MORB > 500 km from a plume-fed hotspot), D-MORB (all MORB with La/Sm_N <0.8) and E-MORB (all MORB with La/Sm_N >0.15) come from Gale *et al*. (2013).

contemporaneous rocks (Figure 5) is more explained by the melting of a compositionally heterogenous mantle source. To discriminate between the importance of the degree of melting and the mantle source, we tested the covariations between Nb/Y and Zr/Y, which have been studied in detail in Icelandic lavas (Fitton *et al*. 1997). This covariation is of global importance and can be used to recognize enriched mantle sources in MORB and OIBs. Low pressure fractional crystallization had no significant effect on these ratios for MgO >5 wt% and various degrees of melting causes covariance along linear arrays parallel to the Iceland array (Figure 8A). Any vertical changes from the array, stated as additional values from the reference pattern of the lower bound of the Iceland array, can be inferred from the source heterogeneity (Fitton *et al*. 1997). This modelling suggests that the studied units were formed from a diverse range of melt compositions, including Nb-depleted to Nd-enriched melts. This geochemical overlap suggests that the magmatic processes that generated the lava, gabbro, and dike are closely intertwined, in agreement with a transitional magmatic system in which the range of melt compositions becomes more enriched over time (Figure 8B). However, despite the irregular differences within each defined subgroup, the mafic dikes are somewhat more LREE enriched (Figure 5E) and Nb/Y-enriched than the other components (Figure 8B), a phenomenon in the Sarv-Abad that is consistent with their observed field relations, where they cross-cut the host lavas and gabbros.

Figure 8 shows that the Sarv-Abad gabbro, lava, and mafic dikes are derived from a source with heterogeneous Nb concentrations. Additionally, the results suggest that more Nb-enriched rock that can be generated by low degrees of partial melting of the enriched component may also contribute to the formation of E-MORB sources. This agrees with previous studies, which show that Sarv-Abad melts are geochemically variable (Ao *et al*. 2016; Ghorbani *et al*. 2022). It has been suggested that melting in the spinel, spinel-garnet transitional, or garnet stability fields generates low Dy/Yb ratios (<1.5), moderate Dy/Yb ratios (1.5–3), and high Dy/Yb (>2.4)

ratios, respectively. The measured Dy/Yb ratio of all basalt, gabbro and mafic rocks in Sarv-Abad are less than 2, which suggests that all mafic rocks formed in the spinel transitional stability field. These rocks with N- and E-MORB characteristics thus partly correspond with suites of the Masirah ophiolite (Oman), as suggested by Jansen *et al*. (2024).

The plagiogranitic dikes are characterized by elevated Zr/Hf ratios (36.0–48.5) that are close to those of typical MORB (33–40) (Büchl *et al*. 2002), but markedly higher than those of average granite (25) (Münker *et al*. 2003), implying a mantle-derived source. Plagiogranites may originate from the fractionation of basaltic magmas (Pedersen and Malpas 1984; Jiang *et al*. 2008) or partial melting of metasomatized gabbros, basalts, or amphibolites (Pedersen and Malpas 1984). Research shows that plagiogranitic melt compositions resulting from fractional crystallization of basaltic magmas differ distinctly from those formed by partial melting of gabbros and amphibolites (Koepke *et al*. 2004), particularly for TiO_2, SiO_2, and K_2O contents. The former model suggests that plagiogranites are extremely fractionated melts generated by the fractionation of parental MORB melt (Coleman and Peterman 1975), whereas the latter model suggests that plagiogranitic melts formed during the partial melting of metasomatized gabbros, caused by the deep infiltration of hydrothermal fluids into the oceanic crust along detachment faults. The Sarv-Abad plagiogranites have a compositional variation that is similar to melts produced by partial melting of metasomatized gabbroic and amphibolitic rocks from the lower oceanic crust (Supplementary Figure S3).

4.2. Temporal evolution of Kurdistan ophiolites

The new U–Pb zircon ages presented here propose a formation age of 38 Ma for gabbros and 41 Ma for plagiogranite dikes from Sarv-Abad (Suppl. Table S4), which correspond to the ages of Sahneh–Kamyaran gabbro from the Kermanshah ophiolite obtained by Ao *et al*. (2016). Previous geochronological studies have suggested two episodes of oceanic crust formation within the KWOC: (1) Late Cretaceous ophiolitic units in the Harsin (Kermanshah), and Razab (Kurdistan), Hassanbang, Mawat, Rayat, Qalender, and (ii) Paleocene-Middle Eocene to Oligocene ophiolitic units in Sarv-Abad, Sahneh, Kamyaran, Walash, and Naupordan. The zircon age of 79.3 ± 0.9 Ma reported by Ao *et al*. (2016) is the best estimate of the crystallization age of the gabbro in the Harsin ophiolite, and these authors also reported DMM and N-MORB signatures for this gabbro. However, the Razab Cretaceous mafic rocks are characterized by basalts with two distinct types, characterized compositionally between depleted MORB mantle (DMM)-N-MORB and OIB field and gabbro with E-MORB and high-Ti N-MORB melts from SSZ environments, supporting magma genesis in a SSZ environment (e.g. Khedr and Arai 2017; Rossetti *et al*. 2017; Saccani *et al*. 2018). In order to evaluate the generation of such magma in the SSZ, a melt curve model was calculated based on La/Yb and Dy/Yb ratios. The previous works show that the melting in the spinel stability field, garnet stability field, or spinel-garnet transitional stability field would produce low Dy/Yb ratios (<1.5), high Dy/Yb ratios (>2.4), and moderate Dy/Yb ratios (1.5–3), respectively. The measured Dy/Yb ratio of most of Cretaceous basaltic and gabbroic rocks in the study area is less than 1.5 (except two OIB-like samples with values of 1.8 and 2.3) and thus supports both (DMM)-N-MORB basalts and EMORB gabbro having been generated in the spinel transitional stability field, whereas those from OIB-like can be formed in the spinel-garnet transitional stability field (e.g. McKenzie and O'Nions 1991). The OIB-like type basaltic rocks from Razab with (av. $(La/Yb)_N = 9.6$ and $(Dy/Yb)_N = 1.93$) may have resulted from partial melting of a mantle source enriched in LREE than garnet bearing spinel lherzolite ($(La/Yb)_N = 0.88$ and $(Dy/Yb)_N = 0.94$) (Figure 9), or else from a very low degree partial melting (<2%) of a DMM source in the spinel-facies. However, low degrees of partial melting of a DMM source in the spinel-facies cannot generate the high $(La/Yb)_N$ and $(Dy/Yb)_N$ ratios in these rocks (not shown). We also note that the La/Yb–Dy/Yb systematics of these rocks are compatible with about low degree partial melting of a garnet bearing spinel lherzolite (i.e. 0.7 gt, 0.3 sp) source (Figure 9). However, DMM-N-MORB basalts and E-MORB gabbro are characterized by lower ($(La/Yb)_N = 0.86$ and $(Dy/Yb)_N = 1.1$) and $(La/Yb)_N = 4.4$ and $(Dy/Yb)_N = 1.1$, in agreement with about high degree partial melting (~20) of a spinel lherzolite (Figure 9).

In contrast, ages of 39–37 Ma have been reported for the Sahneh and Kamyaran gabbros, which are characterized by flat REE patterns and positive Eu anomalies, marked positive Sr anomalies and weak negative anomalies for Nb and Zr. These geochemical features are consistent with those reported from oceanic core complexes like the Atlantis Massif (Boschi *et al*. 2006). Critically, this interpretation is supported by direct structural evidence in Sarv-Abad, including mylonitized gabbros (Figure 4A), serpentinite breccias, and syn-extensional mafic dikes intruding along shear zones, which collectively indicate exhumation via a detachment fault system. Recently, Allahyari *et al*. (2010) reported both E-MORB and N-MORB signatures for gabbros in the Sahneh area. The Eocene gabbros (~38 Ma) in the

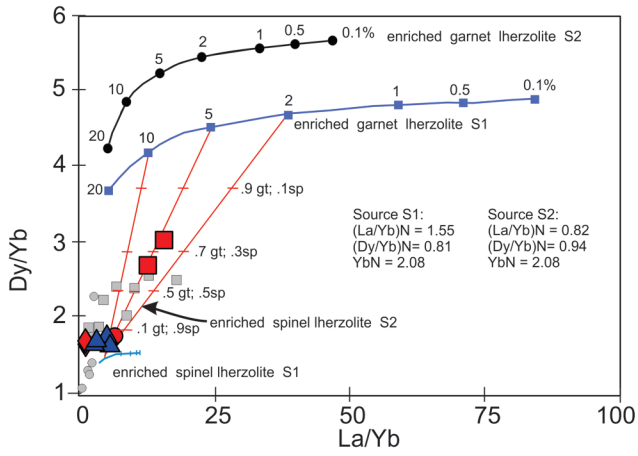

Figure 9. Melt curves are presented for S1 and S2 mantle sources in both garnet and spinel facies, modelled using La/Yb vs. Dy/Yb ratios. The diagram also includes arrays depicting melt mixtures derived from varying proportions of garnet-facies and spinel-facies mantle melts. These curves were generated using non-modal, batch melting models applied to garnet lherzolite (mode: ol 59.8%, opx 21.1%, cpx 7.6%, gt 11.5%; melting proportions: ol 4%, opx −19%, cpx 104%, gt 11%) and spinel lherzolite (mode: ol 57.8%, opx 27.0%, cpx 11.9%, sp 3.3%; melting proportions: ol – 6%, opx 28%, cpx 67%, sp 11%). Mantle source compositions are S1 (Saccani *et al*., 2013a) and S2 (Saccani *et al*., 2013b). Mineral modes and melting proportions follow Kinzler (1997). Normalization uses values from Sun and McDonough (1989).

Sarv-Abad region also show similar geochemical signatures (i.e. REE patterns) and ages to the Sahneh gabbro, although they show no Eu anomalies and are more enriched in Nb. They are compatible with moderate-to-high Ti N-MORB (Saccani *et al*. 2018), and plot in the field of extensional (back-/forearc) basins (Reagan *et al*. 2010).

The Eocene basalts and mafic dikes of Sahneh and Kamyaran show either OIB to E-MORB or calc-alkaline signatures (Whitechurch *et al*. 2013). However, the rocks reported here and basalts reported by Ghorbani *et al*. (2022) suggest two types of lavas with different REE patterns: those weakly depleted in LREE and those with relatively flat REE patterns ($(La/Yb)_N$ values of 0.77–1.24), and weakly LREE-enriched rocks ($(La/Yb)_N$ average = 1.7) which lack an Eu anomaly. Ghorbani *et al*. (2022) indicated that these subgroups show different K–Ar extrusion ages; being Palaeocene–Eocene (59–50 Ma) and Oligocene (29 Ma), respectively. The basalts of this study show depleted to slightly enriched REE pattern with $(La/Yb)_N$ values between 0.8 and 1.8. These values agree with the features reported by Ghorbani *et al*. (2022), and they have no negative Nb or Ti anomalies, indicative of minimal or any role of a subducted-modified mantle source; however, one basaltic sample is characterized by high-Ti, tholeiitic to slight calc-alkaline affinity, similar to those of immature back-arc basins. Consequently, we propose that the Eocene Sarv-Abad basalts were derived from a depleted mantle source situated below an extensional basin above a subduction zone that was weakly metasomatized by fluid from dehydrating crustal materials undergoing prograde metamorphism during subduction.

One undated basaltic sample (this study) along with the Oligocene lavas (29 Ma; Ghorbani *et al*. 2022) shows intermediate tholeiitic to calc-alkaline affinity and are moderately fractionated and characterized by somewhat enriched LREE patterns, signifying lower partial melting degrees in their source region and/or more enrichment in incompatible elements.

It has been proposed that Ba/Nb, Th/Nb, and Ba/Th ratios can be used as tracers to evaluate the contributions of total, deep, and shallow subduction, respectively (Pearce and Stern 2006). Geochemical mapping of subduction input proxies of the Sarv-Abad mafic rocks is characterized by higher Ba/Nb (average = 8.3), Th/Nb (average = 0.08), Ba/Th (average = 94) ratios relative to the average values of these ratios for N-MORB (Ba/Nb = 2.70; Th/Nb = 0.052; Ba/Th = 52.50), respectively (Sun and McDonough 1989), emphasizing the minor role of slab-derived fluid component(s) in the genesis of Sarv-Abad Palaeocene–Eocene extensional basin basalts. The Oligocene basaltic rocks from Sarv-Abad, which were reported by Ghorbani *et al*. (2022), are characterized by higher Ba/Th (59–202) and Ba/Nb (4–31) ratios compared to those of the Palaeocene–Eocene basalts and N-MORB. These authors suggested that the Sarv-Abad Oligocene basalts formed in a more mature back-arc basin. The measured Dy/Yb ratio of Cenozoic basaltic (1.8–2.6) and gabbroic (0.9–2.3) rocks as well as mafic dikes (1.6–1.8) in the Sarv-Abad area is between 1.5 and 3, correspondences with their

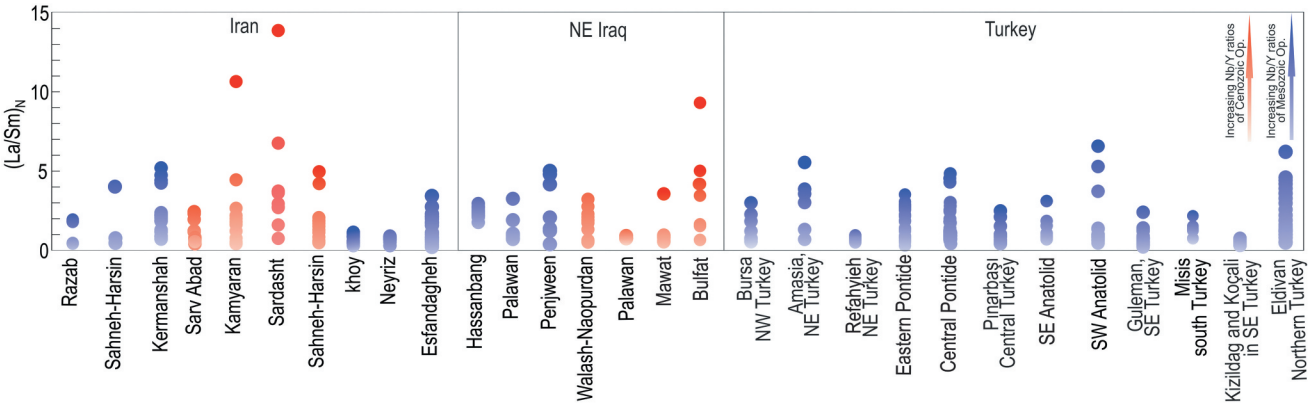

Figure 10. Chondrite-normalized $(La/Sm)_N$ ratios of mafic rocks from the Kurdistan ophiolites (Razab and Sarv-Abad) compared to other Tethyan ophiolites in Iran–Iraq–Turkey (data from Iran come from Ao et al. 2016, 2020; Saccani *et al*. 2014; Ghorbani *et al*. 2022; Whitechurch *et al*. 2013; data from Iraq come from; Ali et al. 2012, 2013; Ali 2015; Gibaga *et al*. 2019, data from Turkey come from Topuz *et al*., 2013; Parlak *et al*., 2009; Sapancı *et al*. 2023; Beyarslan, 2018; Hässig *et al*., 2014). The comparison highlights the depleted, fore-arc affinity of the Cretaceous Razab rocks and the more enriched, extensional back-arc affinity of the Eocene Sarv-Abad rocks.

generation within the spinel–garnet transitional stability field (e.g. McKenzie and O'Nions 1991). The Sarv-Abad E-MORB basalts, gabbro, and mafic dikes are characterized by $(La/Yb)_N = 4.8$ and $(Dy/Yb)_N = 1.4$) and $(La/Yb)_N = 1.21$ and $(Dy/Yb)_N = 0.93$, in agreement with partial melting (~0.5–10) of a spinel lherzolite S2 and high degree partial melting of a garnet bearing spinel lherzolite S1 sources (Figure 9), respectively. While those are the E-MORB, mafic dikes are in agreement with low degree ~0.2–5% partial melting of a garnet bearing spinel lherzolite source for this E-MORB type rocks (Figure 9).

The geochemical signatures of the Kurdistan ophiolites are also consistent with those observed in other Tethyan ophiolitic complexes. Figure 10 compares the La~N~/Sm~N~ ratios of mafic rocks from the Razab and Sarv-Abad sequences with those from key ophiolites in the Peri-Arabian domain, including Sahneh–Harsin, Kamyaran, Walash–Naopurdan, Mawat–Hasanbag, and others from Iran and Iraq (e.g. Aswad *et al*. 2011; Whitechurch *et al*. 2013; Allahyari *et al*. 2014) (Figure 10). The Razab rocks, with their lower LaN~/Sm~N~ values, plot within the field defined by fore-arc and SSZ-type ophiolites, reinforcing their origin during subduction initiation. In contrast, the Sarv-Abad rocks show a broader range extending to higher La~N~/Sm~N~ values, overlapping with the fields of extensional back-arc and oceanic core complex (OCC) settings. This regional comparison underscores the genetic dichotomy between the two units: the Cretaceous Razab ophiolite formed in a nascent arc setting, while the Eocene Sarv-Abad ophiolite records later extension and heterogeneous mantle melting in a back-arc basin, supporting our integrated geochemical and structural model.

4.3. Associations between D-MORB and E-MORB in Sarv-Abad and present-day MORs

This study highlights the difficulty in labelling magmatic systems or mid-ocean ridge/extensional segments as entirely N-MORB, D-MORB, E-MORB, or OIB, and reveals that the compositional evolution of a ridge segment may be complex or change with time. Significantly, the crustal suites defining the Razab and Sarv-Abad ophiolites show that D-MORB, E-MORB, and OIB melts can be extracted from the same heterogeneous mantle system and form basalt, gabbro, and crosscutting dikes during the accretion of oceanic crust. As mentioned above, the changes in melt compositions of the studied basalt and gabbro were derived from variable degrees of partial melting at moderate depths (garnet–spinel field) of a heterogeneous source and were conserved during melt transference and crustal processing.

To test whether the compositional evolution observed at Sarv-Abad is applicable to other MORs worldwide, we examined the compositional variation of MORB within ridge slices using the compilation of Gale *et al*. (2013). Figure 10 displays the La_N/Sm_N and Nb/Y compositions of several MORB slices situated more than 500 km from a hotspot. Most MORB slices range in composition from D-MORB to E-MORB, showing that the variability preserved in Sarv-Abad also occurs along some modern MORs. Furthermore, Nb-enriched compositions (Nb/Y > 0.8, heavy brown symbols; Figure 11) were present in some MORB slices. Studies on modern MORBs have

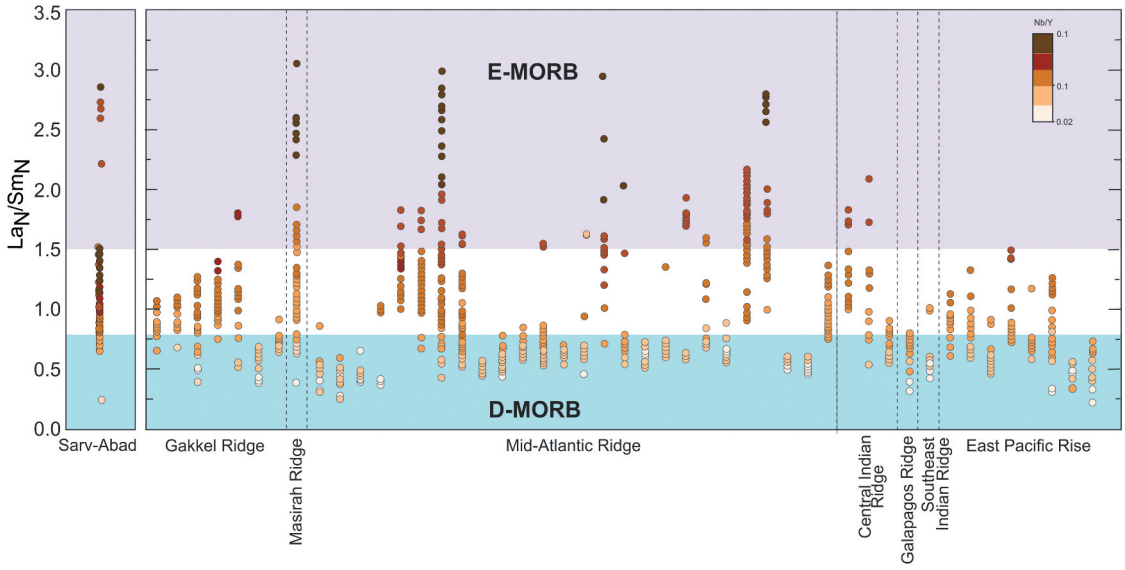

Figure 11. Sarv-Abad lava and dikes La_N/Sm_N compositions (left) compared to present-day MORB variations within individual MOR spreading segments (Gale *et al*. 2013) showing that the wide compositional variability in Masirah is mirrored in certain parts of the slower spread mid-ocean ridge system. MORB data are filtered to exclude segments within 500 km from a plume-fed hotspot as well as segments that have fewer than 10 samples with La/Sm analyses. Data are normalized to primitive mantle (McDonough and Sun 1995) and coloured by Nb/Y content, with star symbols indicating Nb-enriched compositions (Nb/Y >0.8). CIR = Central Indian Ridge, GR = Galapagos Ridge, SEIR = Southeast Indian ridge, SWIR = Southwest Indian Ridge (Modified after Jansen *et al*. 2024).

shown that trace element variations derived from mantle source regions decrease with increasing magma supply and increasing magmatic fractionation (Rubin and Sinton, 2007). In widely spaced magmatic ridge settings, a broader diversity of melt compositions tends to be retained owing to the limited extent of magma mixing. Importantly, the coexistence of D-MORB and E-MORB within a single ridge segment is significantly more frequent in slow-spreading ridges (<~40 mm/year; 10 out of 37 segments, ~27%) than in fast-spreading ridges (>~60 mm/year; 1 out of 10 segments, ~10%), which are characterized by higher magmatic activity. The Sarv-Abad mantle source maintained a well-constrained system that yielded basalts with depleted and enriched composition, and Nb-depleted and Nb-enriched basalts are consistent with a genesis in a plume-unrelated oceanic system, where the heterogeneity originates from recycled crustal components or mantle metasomatism rather than a deep mantle plume (e.g. Hirano *et al*. 2006). These basalts also additionally seem to have a higher potential to preserve their compositions throughout subduction processes, as exemplified by the accretion of trace element enriched seamounts in Costa Rica (Buchs *et al*. 2011) and Anglesey, UK (Saito *et al*. 2015), along with the extensive occurrence of alkali basalts in the Tethyan realm (e.g. the Haybi volcanics beneath the Semail Ophiolite nappe in the northern Oman; Searle *et al*. 1980). Although there are differences in tectonic settings, some of these rocks seem to have geochemical similarities, elevated Nb/Y (>0.7) and $(La/Sm)_N$ (>1.5) ratios, in terms of formation by low degrees of melting of an enriched mantle source (e.g. Fitton *et al*. 1997).

Our work shows that such rocks do not need a deep mantle source and can, alternatively, be generated during different partial melting of the same heterogeneous mantle that underlies the extensional slow-spreading ridge.

4.4. Tectonic evolution model

The Iranian plate rifted from the Arabian plate as a micro-continental fragment in response to the opening of Neo-Tethys oceanic lithosphere during the Late Triassic (Agard *et al*. 2005, 2011; Moghadam *et al*. 2015) (Figure 12A). This was followed by subduction initiation of the Neo-Tethys beneath the Iranian plate during the Late Jurassic–Early Cretaceous (Ghasemi and Talbot 2006; Moghadam and Stern 2021), leading to the formation of low- to medium-pressure metamorphism within the Sanandaj–Sirjan Zone and the associated Neo-Tethyan suture. We suggest that interoceanic subduction initiation plays a critical role in the formation of the Late Cretaceous KWOC ophiolites, including those in the Kurdistan ophiolite. This process involves the onset of subduction in a previously passive or extensional tectonic setting (Figure 12B). Therefore, during the Late Cretaceous, the Neo-Tethys Ocean was progressively narrowing due to convergence between the Arabian and Iranian plates. Subduction initiation often occurs at

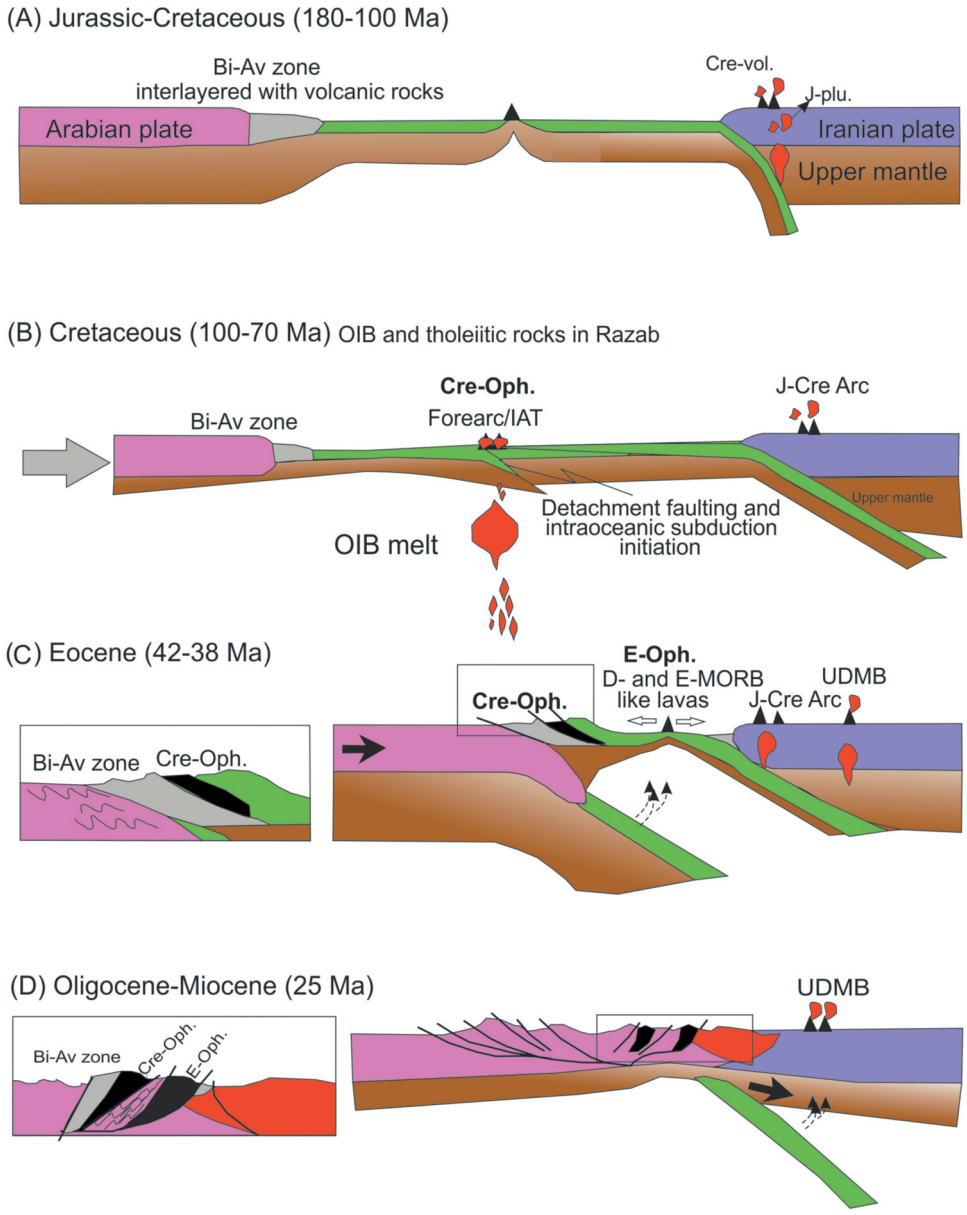

Figure 12. Schematic model for tectono-magmatic evolution and genesis of two parallel Late Mesozoic and Cenozoic ophiolites of NW Iran. Bi-av: Bisotun-Avroman; cre-vol: Cretaceous volcanic rocks; J-Plu.: Jurassic plutonic rocks; cre-Oph.: Cretaceous ophiolite; J-Cre arc: Jurassic–Cretaceous arc; E-Oph.: Eocene ophiolite. (A) Iranian plate rifted as a micro-continental fragment from the Arabian plate, in response to the Neo-Tethys oceanic lithosphere opening during the Late Triassic. (B) Due to convergence forces, intra-oceanic subduction initiated through the Zagros suture zone, leading to the formation of mafic rocks with MORB and supra-subduction affinity. (C) In the Early Cenozoic, during continued conversion forces, Cretaceous ophiolites obducted on the Arabian plate, the rollback of Neo-Tethys occurred, and an extensional tectonic setting occurred leading to the formation of detachment faulting and replacement of Cenozoic magmatic rocks related to young ophiolites. (D) In continuous with the closure of Neo-Tethys, both two ophiolitic rocks close to each other are emplaced onto the continent.

pre-existing zones of lithospheric weakness (e.g. Stern 2004), leading to the formation of forearc/island arc magmatism (Figure 12B). High-temperature/low-pressure conditions in the forearc and island arc environments lead to upwelling and decompression melting, resulting in a layered structure of ophiolites (peridotites, gabbro, dike complexes, and pillow lavas) (Figure 12B). Following their formation, these ophiolites were emplaced onto the continental margin during continued plate convergence, marking a transition from oceanic to continental tectonic environments (Figure 12C). This model is confirmed by the SSZ signatures of Kurdistan Cretaceous ophiolite igneous rocks, particularly for mantle peridotite (Nouri *et al*. 2018), and by the existence of early MORB-like and OIB-like lavas (basalts) in some of these ophiolites, which are succeeded by more arc-like

magma (gabbro) (Whattam and Stern 2011). These are the mantle expressions of subduction initiation, as documented in several well-known ophiolite volcanic sections by Whattam and Stern (2011), whereby subduction initiation is manifested by the early expression of tholeiitic basalts in the forearc. Upwelling of the asthenospheric (OIB-like) mantle beneath the forearc region during the early stages of subduction initiation first resulted in decompression melting in the FAB (Reagan *et al*. 2010). Such melts crystallized spinel with compositions similar to those of chromities and the OIB-like basalts in Kurdistan. These FAB melts were also followed by the generation of arc-like melts as slab-derived fluids intruded into the zone of melt generation in the mantle wedge as the sinking slab descended further. These later arc-like melts formed the Mesozoic enriched tholeiitic basalts and calc-alkaline gabbro of Kurdistan (Figure 12C).

The formation of magmatic rocks exposed on the Sarv-Abad ophiolite took place at 59 Ma (Ghorbani *et al*. 2022) extended to the Eocene (41–36 Ma; this study) and the latest magmatic activity occurred in the Oligocene (~29 Ma, Ghorbani *et al*. 2022). U–Pb dating of gabbros and plagiogranites (~42–38 Ma; this study) (Figure 7) and basaltic rocks (59–29 Ma; Ghorbani *et al*. 2022) indicate that the crustal section of Sarv-Abad is part of the Cenozoic magmatic slices of Kurdistan ophiolite. Sarv-Abad peridotites exhibit Cr# values of 0.58–0.69 and variable Mg# (0.48–0.65), which are lower than those typical of highly depleted forearc peridotites and instead fall within the range of moderately depleted abyssal and back-arc peridotites. This moderate depletion is indicative of heterogeneous mantle melting in an extensional back-arc setting, rather than in a mature arc. These mineral-chemical signatures correlate with (i) Syn-extensional detachment faulting evidenced by mylonitized gabbros (Figure 4A), and peridotites, mesh-textured serpentinized peridotites (Figure 4E), the presence of serpentinite-breccia zones interpreted as fault gouge, the occurrence of syntectonic mafic dikes intruding along shear zones, the overall tectonic slicing of lower crustal and mantle sequences mylonitized gabbros and normal faults transecting ultramafic units; (ii) contemporaneous E-MORB/D-MORB magmatism (Figure 5); (iii) hydrothermal metasomatism reflected in LILE-enriched mafic rocks (e.g. Ba/Th ≈ 94); (iv) plagiogranites with negative Eu anomalies (Eu/Eu* = 0.3–0.6) and HFSE depletion. Collectively, these features diagnose Oceanic Core Complex (OCC) formation, analogous to the Atlantis Massif (Pressling *et al*. 2012).

Detachment faulting model for the Sarv-Abad ophiolite fundamentally reinterprets the geodynamic evolution of the KWOC. It resolves key prior ambiguities, namely: (1) the conflicting interpretations of a purely subduction-related (SSZ) origin versus an extensional origin for the peridotites and gabbros and (2) the mechanism and timing of their exhumation. While Allahyari *et al*. (2014) interpreted Sarv-Abad peridotites as products of SSZ melting based on their refractory compositions (high Mg# = 0.88–0.91), we demonstrate, through structural evidence (mylonitized gabbros, normal faults, and serpentinite breccias; Figure 4), that these units were exhumed via detachment faulting in an oceanic core complex (OCC) setting. The contemporaneous D-MORB and E-MORB magmatism further contradicts pure SSZ models, requiring heterogeneous mantle melting during extension rather than subduction-dominated processes.

Although Ao *et al*. (2016) pioneered the OCC model for Eocene Sahneh–Kamyaran gabbros (~36 Ma), our study provides the first structural and geochemical evidence that this mechanism operated in the Sarv-Abad (U–Pb ages: 42–38 Ma). Critically, we also demonstrate that mantle heterogeneity – not plume influence – explains contemporaneous D-MORB/E-MORB magmatism during OCC formation. Our OCC framework accounts for this duality through low-degree melting of heterogeneous mantle during lithospheric extension, consistent with global OCC systems like the Atlantis Massif. This E-MORB/D-MORB coexistence, OCC formation, and moderate Ba/Th (avg. 94) align with back-arc extension (e.g. Pearce and Stern 2006).

Thus, a comparison of the Sarv-Abad ophiolite with the structure and life cycle of modern *in situ* OCCs enables us to propose a new scenario to explain the observed heterogeneity of the Sarv-Abad ophiolite. Here, we tested two different mechanisms that may clarify the observed evolution of the Sarv-Abad magmatic unit. The first mechanism involves the occurrence of trace element-enriched melts and the progressive increase in trace element enrichment over time may be related to the effect of magmatism related to hotspot (e.g. Meyer *et al*. 1996). Although hotspots characteristically cause trace element enrichment in the OIB and E-MORB in regions of hotspot–ridge interaction, their REE patterns are typically HREE depleted due to melting in the garnet stability field. The lack of HREE depletion in Sarv-Abad magmas is inconsistent with deep melting (Figure 5G). Furthermore, the absence of seamount lavas in Sarv-Abad argues against a hotspot origin or influence since hotspots tend to be places of enhanced melting. It is also confirmed by low Ba/Nb (avg. 8.3) and Th/Nb (avg. 0.08) ratios which fall within MORB–back-arc ranges (Sun and McDonough 1989), distinct from plume-influenced settings (e.g. Hawaii: Ba/Nb > 100; Hofmann 1997). The second scenario is that they can be produced from the same heterogeneous source that generated the

melts and showed a similarity with basalts from Masirah Island. The formation of Masirah Island records ridge magmatism ending and a change in plate motions that occurred in the Indian Ocean a ~135–130 Ma, which contributed to the termination of seafloor spreading at the Masirah palaeoridge.

In this scenario, the first stage involved the intrusion of N-MORB basaltic rocks into the upper mantle (ca. 52 Ma), which affected the rheology of the upper mantle, weakening it by the spread of fracture networks and hydrothermal circulation. The second stage was characterized by large-scale detachment faulting that developed within the serpentinized front of the upper mantle (ca. 38 Ma). The extension induced by slab rollback was a critical factor for the initiation of detachment faulting (Figure 11D). The third stage was characterized by syn-extensional magmatism associated with the development of detachment fault. Invasion of mafic dikes into the upper part of the Sarv-Abad suggests that the active detachment fault was the main magma conduit during this stage. The detachment faulting evolved to its last stage following the exhumation of the extensive syn-extensional serpentinite breccias that were emplaced in the sheared serpentinite. Thus, we suggest that the life cycle of the Sarv-Abad ophiolite is a combination of tectonic and magmatic processes. Our new model provides an explanation for other ophiolites in the KWOC, specifically, many ophiolites with similar emplacement ages (ca. 79–38 Ma). Most KWOC have large ultramafic massifs crosscut by various mafic dikes (Whitechurch *et al*. 2013; Ao *et al*. 2016). Dick *et al*. (2008) described similar off-axis magmatism along the OCC and suggested that this is a common phenomenon.

5. Conclusions

(1) U–Pb dating of zircons shows that magmatism on Sarv-Abad occurred during the Eocene, as previously reported. Two crosscutting intrusions yielded ages of ~42–38 Ma, overlapping with the proposed Eocene emplacement age of the Kermanshah-Walash ophiolites. In contrast, the radiolarites from the Razab ophiolite contain radiolarians and a large amount of sponge spicules that are Cretaceous in age.

(2) The geochemical characteristics of mafic igneous rocks from the Razab Cretaceous ophiolite suggest petrogenetic evolution from early-stage low-Ti IAT-like basalts to later-stage high-Ti E-MORB-like gabbro progressively less-affected by subduction-derived components and also containing OIB-like basalts. The Sarv-Abad igneous crust was generated by contemporaneous D-MORB and E-MORB magmatism formed by melting a heterogeneous mantle, whereas later stages revealed an increasing contribution of low-degree spinel-garnet stability field melting of the enriched component in the source. The substantial similarity in the trace element compositions of the mafic dikes and lava units suggests that they formed during a transitional magmatic event where the main phase of the crust was accreted.

(3) The trace element compositions of gabbro and lava from the Razab ophiolite indicate formation from tholeiitic melts generated during early proto-forearc/island arc spreading during subduction initiation, while those of the lava and dikes from the Sarv-Abad ophiolite may have been formed via different degrees partial melting of the same heterogeneous source that generated the axial melts of the extensional spreading centre.

(4) The Kurdistan ophiolite components experienced ductile and brittle deformation along the extensional detachment faults that occurred in Sarv-Abad and Kamyaran. Consequently, we suggest that the Sarv-Abad, Sahneh, Kamyaran part of the Kurdistan and Kermanshah ophiolites were possibly an oceanic core complex generated by large oceanic detachment faults at ca. 40–38 Ma.

Acknowledgements

This paper is part of a project of the first author. We gratefully acknowledge Prof. Jamshid Hassanzadeh for providing financial support for the dating analyses. We thank Prof. Robert J. Stern for editorial handling and Dr. Tehseen Zafar and anonymous reviewer for constructive comments and suggestions, allowing us to greatly improve the manuscript. The first and second author acknowledges support from Shahid Beheshti University and Ferdowsi University of Mashhad, respectively, for assistance during fieldwork. BR acknowledges funds #3471 supported by Shahid Beheshti University, Tehran, Iran.

Disclosure statement

We declare that we have no known competing financial interests or personal relationships that could have appeared to influence the work reported in this paper.

Funding

The author(s) reported there is no funding associated with the work featured in this article.

Author contributions statement

Dr. Bahman Rahimzadeh contributed to the design and implementation of the research, to the analysis of the results, performed the experiments, derived the analysed the data, and to the writing of the manuscript.
Dr. Fatemeh Sepidbar contributed to the design of ideas, devised the project, the main conceptual ideas, proof outline, implementation of the research, and to the writing of initial version of the manuscript.
Prof. Harald Furnes contributed to the design of ideas, interpretation of the data, and to the revising scientific issues of initial version of the manuscript.
Prof. Richard M. Palin contributed to the revising of scientific issues of initial version of the manuscript.

References

Agard, P., Jolivet, L., Vrielynck, B., Burov, E., and Monie, P., 2007, Plate acceleration: The obduction trigger?: Earth and Planetary Science Letters, v. 258, p. 428–441. doi: 10.1016/j.epsl.2007.04.002

Agard, P., Omrani, J., Jolivet, L., and Mouthereau, F., 2005, Convergence history across Zagros (Iran): Constraints from collisional and earlier deformation: International Journal of Earth Sciences, v. 94, no. 3, p. 401–419. doi: 10.1007/s00531-005-0481-4

Agard, P., Omrani, J., Jolivet, L., Whitechurch, H., Vrielynck, B., Spakman, W., Monie, P., Meyer, B., and Wortel, R., 2011, Zagros orogeny: A subduction-dominated process: Geological Magazine, v. 148, no. 5–6, p. 692–725. doi: 10.1017/s001675681100046x

Ahmadipour, H., and Rostamizadeh, G., 2012, Geochemical aspects of Na-metasomatism in Sargaz granitic intrusion (South of Kerman Province, Iran): Journal of Sciences, Islamic Republic of Iran, v. 23, p. 45–58.

Ali, S.A., 2015, Petrogenesis of metabasalt rocks in the Bulfat complex, Kurdistan region, Iraqi Zagros suture zone: Kirkuk University Journal-Scientific Studies, v. 10, no. 3, p. 242–252. doi: 10.32894/kujss.2015.104996

Ali, S.A., Buckman, S., Aswad, K.J., Jones, B.G., Ismail, S.A., and Nutman, A.P., 2012, Recognition of Late Cretaceous Hasanbag ophiolite-arc rocks in the Kurdistan region of the Iraqi Zagros suture zone: A missing link in the paleogeography of the closing Neotethys ocean: The Geological Society of America, Lithosphere, v. 4, no. 5, p. 395–410. doi: 10.1130/L207.1

Ali, S.A., Buckman, S., Aswad, K.J., Jones, B.G., Ismail, S.A., and Nutman, A.P., 2013, Thetectonic evolution of a Neo-Tethyan (Eocene–Oligocene) island-arc (Walash and Naopurdan groups) in the Kurdistan region of the northeast Iraqi Zagros suture zone: Island Arc, v. 22, p. 104–125. doi: 10.1111/iar.12007

Allahyari, K., Saccani, E., Pourmoafi, M., Beccaluva, L., and Masoudi, F., 2010, Petrology of mantle peridotites and intrusive mafic rocks from the Kermanshah ophiolitic complex (Zagros belt, Iran): Implications for the geodynamic evolution of the Neo-Tethyan oceanic branch between Arabia and Iran: Ofioliti, v. 35, p. 71–90.

Allahyari, K., Saccani, E., Rahimzadeh, B., and Otavia, Z., 2014, Mineral chemistry and petrology of highly magnesian ultramafic cumulates from the Sarve-Abad (sawlava) ophiolites (Kurdistan, NW Iran): New evidence for boninitic magmatism in intra-oceanic fore-arc setting in the Neo-Tethys between Arabia and Iran: Journal of Asian Earth Sciences, v. 79, p. 312–328.

Ao, S., Mao, Q., Xiao, W., Khalatbari Jafari, M., Windley, B.F., Song, D., Zhang, Z., Zhang, J., Wan, B., Han, C., and Xiao, W., 2020, U–Pb age, Hf–O isotopes, and geochemistry of the Sardasht ophiolite in the NW Zagros orogen: Implications for the tectonic evolution of Neo-Tethys. doi: 10.1002/gj.4011

Ao, S., Xiao, W., Khalatbari Jafari, M., Talebian, M., Chen, L., Wan, B., and Zhang, Z., 2016, U–Pb zircon ages, field geology and geochemistry of the Kermanshah ophiolite (Iran): From continental rifting at 79 Ma to oceanic core complex at ca. 36 Ma in the southern Neo-Tethys: Gondwana Research, v. 31, p. 305–318. doi: 10.1016/j.gr.2015.01.014

Arai, S., 1994, Characterization of spinel peridotites by olivine-spinel compositional relationships: Review and interpretation: Chemical Geology, v. 113, no. 3–4, p. 191–204. doi: 10.1016/0009-2541(94)90066-3

Arvin, M., and Robinson, P.T., 1994, The petrogenesis and tectonic setting of lavas from the baft ophiolitic mélange, southwest of Kerman, Iran: Canadian Journal of Earth Sciences, v. 31, p. 824–834. doi: 10.1139/e94-076

Aswad, K.J.A., Aziz, N.R.H., and Koyi, H.A., 2011, Cr-spinel compositions in serpentinites and their implications for the petrotectonic history of the Zagros suture zone, Kurdistan region, Iraq: Geological Magazine, v. 148, no. 5–6, p. 802–818. doi: 10.1017/S0016756811000422

Barnes, J.D., Beltrando, M., Lee, C.T.A., Cisneros, M., Loewy, S., and Chin, E., 2014, Geochemistry of Alpine serpentinites from rifting to subduction: A view across paleogeographic domains and metamorphic grade: Chemical Geology, v. 389, p. 29–47. doi: 10.1016/j.chemgeo.2014.09.012

Batiza, R., and Niu, Y., 1992, Petrology and magma chamber processes at the east pacific rise ~9°30′N: Journal of Geophysical Research, v. 97, no. B5, p. 6779–6797. doi: 10.1029/92JB00172

Berberian, F., and Berberian, M. 1981. Tectono-plutonic episodes in Iran, *in* Frances M. Delany, Harsh K. Gupta (Eds.), Zagros, Hindu Kush, Himalaya: Geodynamic Evolution: Washington, DC, AGU, p. 5–32. doi: 10.1029/GD003p0005.

Beyarslan, M., and Bingöl, A.F., 2018, Zircon U-Pb age and geochemical constraints on the origin and tectonic implications of late Cretaceous intra-oceanic arc magmatics in the Southeast Anatolian Orogenic Belt (SE-Turkey). Journal of African Earth Sciences, v. 147, p. 477–497.

Boschi, C., Früh-Green, G.L., Delacour, A., Karson, J.A., and Kelley, D.S., 2006, Mass transfer and fluid flow during detachment faulting and development of an oceanic core complex, Atlantis Massif (MAR 30°N). Geochemistry, Geophysics, Geosystems, v. 7, no. 1. doi: 10.1029/2005GC001074

Braud, J., 1987, La suture du Zagros au niveau de Kermanshah (Kurdistan iranien): reconstitution paléogéographique, évolution géodynamique, magmatique et structurale. Unpublished doctoral dissertation. Univ. Paris-Sud, Orsay, p 439.

Büchl, A., Brügmann, G., Batanova, V.G., Münker, C., and Hofmann, A.W., 2002, Melt percolation monitored by Os isotopes and HSE abundances: A case study from the mantle section of the troodos ophiolite: Earth and Planetary Science

Letters, v. 204, no. 3–4, p. 385–402. doi: 10.1016/s0012-821x(02)00977-9

Buchs, D.M., Arculus, R.J., Baumgartner, P.O., and Ulianov, A., 2011, Oceanic intraplate volcanoes exposed: Example from seamounts accreted in Panama: Geology, v. 39, no. 4, p. 335–338. doi: 10.1130/G31703.1

Coleman, R.G., and Peterman, Z.E., 1975, Oceanic plagiogranite: Journal of Geophysical Research, v. 80, no. 8, p. 1099–1108. doi: 10.1029/jb080i008p01099

Delaloye, M., and Desmons, J., 1980, Ophiolites and melange terranes in Iran: A geochronological study and its paleotectonic implications: Tectonophysics, v. 68, no. 1–2, p. 83–111. doi: 10.1016/0040-1951(80)90009-8

Deschamps, F., Godard, M., Guillot, S., and Hattori, K., 2013, Geochemistry of subduction zone serpentinites: A review: Lithos, v. 178, p. 96–127. doi: 10.1016/j.lithos.2013.05.019

Dick, H.J.B., Tivey, M.A., and Tucholke, B. E., 2008, Plutonic foundation of a slow-spreading ridge segment: Oceanic core complex at Kane Megamullion, 23°30′N, 45°20′W: Geochemistry, Geophysics, Geosystems, v. 9, no. 5, p. Q05014. doi: 10.1029/2007GC001645

Dilek, Y., and Furnes, H., 2011, Ophiolite genesis and global tectonics: Geochemical and tectonic fingerprinting of ancient oceanic lithosphere: Geological Society of America Bulletin, v. 123, p. 387–411. doi: 10.1130/B30446.1

Dilek, Y., and Furnes, H., 2014, Ophiolites and their origins: Elements, v. 10, no. 2, p. 93–100. doi: 10.2113/gselements.10.2.93

Dilek, Y., and Yang, J.-S., 2018, Ophiolites, diamonds, and ultrahigh-pressure minerals: Discoveries and concepts on upper mantle petrogenesis: Lithosphere, v. 10, no. 1, p. 3–13. doi: 10.1130/L715.1

Fitton, J.G., Saunders, A.G., Norry, M.J., and Hardarson, B.S., 1997, Thermal and chemical structure of the Iceland plume: Earth and Planetary Science Letters, v. 153, no. 3–4, p. 197–208. doi: 10.1016/S0012-821X(97)00170-2

Furnes, H., and Dilek, Y., 2022, Archean versus Phanerozoic oceanic crust formation and tectonics: Ophiolites through time: Geosystems and Geoenvironment, v. 1, no. 1, p. 100004. doi: 10.1016/j.geogeo.2021.09.004

Furnes, H., Robins, B., and de Wit, M., 2012, Geochemistry and petrology of lava in the upper onverwacht suite, Barberton Mountain Land, South Africa: South African Journal of Geology, v. 115, no. 2, p. 171–210. doi: 10.2113/gssajg.115.2.171

Gale, A., Dalton, C.A., Langmuir, C.H., Su, Y., and Schilling, J.G., 2013, The mean composition of ocean ridge basalts: Geochemistry, Geophysics, Geosystems, v. 14, no. 3, p. 489–518. doi: 10.1029/2012GC004334

Ghasemi, A., and Talbot, C.J., 2006, A new tectonic scenario for the Sanandaj–Sirjan Zone (Iran: Journal of Asian Earth Sciences, v. 26, no. 6, p. 683–693. doi: 10.1016/j.jseaes.2005.01.003

Ghorbani, M.R., Mahmoudi, H., Sepidbar, F., and Barth, M., 2022, Geochemical and geochronological constraints on origin of the sawlava ophiolite (NW Iran): Evidence for oceanic mantle evolution beneath Iran-Iraq border: Lithos, v. 418, no. 419, p. 106695. doi: 10.1016/j.lithos.2022.106695

Gibaga, C.R.L., Arcilla, C.A., and Hoang, N., 2019, Volcanic rocks from the central and southern Palawan ophiolites, Philippines: Tectonic and mantle heterogeneity constraints: Journal of Asian Earth Sciences: X, v. 4, p. 103968. doi: 10.1016/j.jaesx.2020.100038

Gillis, K.M., and Thompson, G., 1993, Metabasalt from the mid-Atlantic Ridge: New insight into hydrothermal systems in slow-spreading crust: Contributions to Mineralogy and Petrology, v. 113, no. 4, p. 502–523. doi: 10.1007/BF00698319

Hart, S.R., and Zindler, A., 1986, In search of a bulk-earth composition: Chemical Geology, v. 57, no. 3–4, p. 247–267. doi: 10.1016/0009-2541(86)90053-7

Hässig, M., Rolland, Y., Sosson, M., Galoyan, G., Sahakyan, L., and Topuz, G., 2014, Linking the NE Anatolian and lesser caucasus ophiolites: Evidence for large-scale obduction of oceanic crust and implications for the formation of the lesser caucasus–pontides arc: Geodinamica Acta, v. 26, no. 3–4, p. 311–330. doi: 10.1080/09853111.2013.877236

Hastie, A.R., Kerr, A.C., Pearce, J.A., and Mitchell, S.F., 2007, Classification of altered volcanic island arc rocks using immobile trace elements: Development of the Th–co discrimination diagram: Journal of Petrology, v. 48, p. 2341–2357. doi: 10.1093/petrology/egm062

Hirano, N., Takahashi, E., Yamamoto, J., Abe, N., Ingle, S.P., and Kaneoka, I. 2006, Volcanism in response to plate flexure: Science, v. 313, no. 5792, p. 1426–1428. doi: 10.1126/science.1128235

Hofmann, A.W., 1997, Mantle geochemistry: The message from oceanic volcanism: Nature, v. 385, p. 219–229. doi: 10.1038/385219a0

Hofmann, A., and Wilson, A.H., 2007, Silicified basalts, bedded cherts and other sea floor alteration phenomena of the 3.4 Ga Nondweni Greenstone belt, South Africa, *in* Van Kranendonk, M.J., Smithies, R.H., and Bennett, V.C., eds. Earth's oldest rocks: Development in precambrian geology: Vol. 15, pp. 571–605. doi: 10.1016/S0166-2635(07)15055-6

Ishii, T., Robinson, P.T., Maekawa, H., and Fiske, R., 1992, Petrological studies of peridotites from diapiric serpentinite seamounts in the izu-ogasawara-Mariana forearc, leg 125. In: Proceedings of the Ocean Drilling Program, Scientific Results, 125. Ocean Drilling Program, College Station, TX, pp. 445–485.

Jansen, M.N., MacLeod, C.J., Lissenberg, C.J., Parkinson, I.J., and Condon, D.J., 2024, Relationship between D-MORB and E-MORB magmatism during crustal accretion at mid-ocean ridges: Evidence from the Masirah ophiolite (Oman): Geochemistry, Geophysics, Geosystems, v. 25, no. 3, Article e2023GC011361. doi: 10.1029/2023GC011361

Jiang, Y.H., Liao, S.Y., Yang, W.Z., and Shen, W-Z., 2008, An island arc origin of plagiogranites at Oytag, western Kunlun Orogen, Northwest China: SHRIMP zircon U-Pb chronology, elemental and Sr-Nd-Hf isotopic geochemistry and paleozoic tectonic Implications: Lithos, v. 106, no. 3–4, p. 323–335. doi: 10.1016/j.lithos.2008.08.004

Khedr, M.Z., and Arai, S., 2017, Peridotite-chromitite complexes in the Eastern Desert of Egypt: Insight into neoproterozoic sub-arc mantle processes: Gondwana Research, v. 52, p. 59–79. doi: 10.1016/j.gr.2017.09.001

Khedr, M.Z., Arai, S., and Python, M., 2013, Petrology and chemistry of basal lherzolites above the metamorphic sole from Wadi Sarami, Central Oman ophiolite: Journal of Mineralogical and Petrological Sciences, v. 108, no. 1, p. 13–24. doi: 10.2465/jmps.121026

Khedr, M.Z., Arai, S., Python, M., and Tamura, A., 2014, Chemical variations of abyssal peridotites in the Central Oman ophiolite: Evidence of oceanic mantle heterogeneity: Gondwana Research, v. 25, p. 1242–1262. doi: 10.1016/j.gr.2013.05.010

Kinzler, R.J., 1997, Melting of mantle peridotite at pressures approaching the spinel to garnet transition: Application to mid-ocean ridge basalt petrogenesis: Journal of Geophysical Research, v. 102. no. B1, p. 853–874.

Koepke, J., Feig, S.T., Snow, J., and Freise, M., 2004. Petrogenesis of oceanic plagiogranites by partial melting of gabbros: An experimental study. Contrib. Mineral. Petrol., v. 146, no. 4, p. 414–432.

Koshnaw, R.I., Horton, B.K., Stockli, D.F., Barber, D.E., Tamar-Agha, M.Y., and Kendall, J.J., 2017, Neogene shortening and exhumation of the zagros fold-thrust belt and foreland basin in the Kurdistan region of northern Iraq: Tectonophysics, v. 694, p. 332–355. doi: 10.1016/j.tecto.2016.11.016

Lázaro, C., Blanco-Quintero, I.F., Proenza, J.A., Rojas-Agramonte, Y., Neubauer, F., Núñez-Cambra, K., and Garcia-Casco, A. 2016. Petrogenesis and $^{40}ar/^{39}ar$ dating of proto-forearc crust in the early cretaceous caribbean arc: The La tinta mélange (eastern Cuba) and its easterly correlation in Hispaniola: International Geology Review, v. 58, no. 8, p.1020–1040. doi: 10.1080/00206814.2015.1118647

LeMaitre, R.W., Streckeisen, A., Zanettin, B., Le Bas, M.J., Bonin, B., Bateman, P., Bellieni, G., Dudek, A., Efremova, S., Keller, J., Lameyre, J., Sabine, P.A., Schmid, R., Sqrensen, H., and Woolley, A.R., 2002 , Igneous rocks. A classification and glossary of terms, *in* Le Maitre, R.W., ed. Recommendations of the IUGS subcommission on the systematics of igneous rocks: Cambridge University Press, England, p. 236.

Lian, D., Yang, J., Dilek, Y., and Rocholl, A., 2019, Mineralogy and geochemistry of peridotites and chromitites in the aladag ophiolite (Southern Turkey): Melt evolution of the Cretaceous neotethyan mantle: Journal of the Geological Society, v. 176, no. 5, p. 958–974. doi: 10.1144/jgs2018-060

Maruyama, S., Liou, J.G., and Terbayashi, M., 1996, Blueschist and eclogites of the world, and their exhumation: International Geology Review, v. 38, no. 6, p. 485–594. doi: 10.1080/00206819709465347

McDonough, W.F., and Sun, S.S., 1995, The composition of the Earth: Chemical Geology, v. 120, p. 223–253. doi: 10.1016/0009-2541(94)00140-4

Meyer, J., Mercolli, I., and Immenhauser, A., 1996, Off-ridge alkaline magmatism and seamount volcanoes in the Masirah island ophiolite, Oman: Tectonophysics, v. 267, no. 1–4, p. 187–208. doi: 10.1016/S0040-1951(96)00094-7

Moghadam, H.S., 2009, The nain-baft Ophiolites (central Iran): Age, structure and origin [Ph.D. thesis]: Tehran, Iran, Shahid Beheshti University, p. 532.

Moghadam, H.S., Li, X.-H., Ling, X.-X., Stern, R.J., Khedr, M.Z., Chiaradia, M., Ghorbani, G., Arai, S., and Tamura, A., 2015, Devonian to Permian evolution of the Paleo-Tethys ocean: New evidence from U–Pb zircon dating and Sr–Nd–Pb isotopes of the darrehanjir–Mashhad "ophiolites", NE Iran: Gondwana Research, v. 28, no. 2, p. 781–799. doi: 10.1016/j.gr.2014.06.009

Moghadam, H.S., and Stern, R.J., 2014, Ophiolites of Iran: Keys to understanding the tectonic evolution of SW Asia: (I) Paleozoic ophiolites: Journal of Asian Earth Sciences, v. 91, p. 19–38. doi: 10.1016/j.jseaes.2014.04.008

Moghadam, H.S., and Stern, R.J., 2021, Subduction initiation causes broad upper plate extension: The Late Cretaceous Iran example: Lithos, v. 398-399, p. 398–399, p.106296. doi: 10.1016/j.lithos.2021.106296

Moores, E.M., 1983, Origin and emplacement of ophiolites: Reviews of Geophysics, v. 20, no. 4, p. 735–760. doi: 10.1130/0016-7606(1999)111<1192:SAPOTO>2.3.CO;2.

Münker, C., Pfänder, J.A., Weyer, S., Büchl, A., Kleine, T., and Mezger, K., 2003. Evolution of planetary cores and the Earth-Moon system from Nb/Ta systematics: Science, v. 301, no. 5629, p. 84–87. doi: 10.1126/science.1084662

Niu, Y., and Batiza, R., 1997, Trace element evidence from seamounts for recycled oceanic crust in the Eastern Pacific mantle: Earth and Planetary Science Letters, v. 148, no. 3–4, p. 471–483. doi: 10.1016/S0012-821X(97)00048-4

Nouri, F., Asahara, Y., Azizi, H., and Tsuboi, M., 2018, Petrogenesis of the Harsin-Sahneh serpentinized peridotites along the Zagros suture zone, western Iran: New evidence for mantle metasomatism due to oceanic slab flux: Geological Magazine, v. 156, no. 5, p. 772–800. doi: 10.1017/S0016756818000201

O'Neill, H.S.C., and Jenner, F.E., 2012, The global pattern of trace-element distributions in ocean floor basalts: Nature, v. 491, p. 698–704. doi: 10.1038/nature11678

Pagé, P., Bédard, J.H., Schroetter, J.M., and Tremblay, A., 2008, Mantle petrology and mineralogy of the thetford mines ophiolite complex: Lithos, v. 100, no. 1–4, p. 255–292. doi: 10.1016/j.lithos.2007.06.017

Parkinson, I.J., and Pearce, J.A., 1998, Peridotites from the Izu–Bonin–Mariana forearc (ODP leg 125): Evidence for mantle melting and melt–mantle interaction in a suprasubduction zone setting: Journal of Petrology, v. 39, no. 9, p. 1577–1618. doi: 10.1093/petroj/39.9.1577

Parlak, O., Rızaoğlu, T., Bağcı, U., Karaoğlan, F., and Höck, V., 2009. Tectonic significance of the geochemistry and petrology of ophiolites in southeast Anatolia, Turkey: Tectonophysics, v. 473, no. 1–2, p. 173–187. doi: 10.1016/j.tecto.2008.08.002

Pearce, J.A., 1996, A users guide to basalt discrimination diagrams, *in* Wyman, D.A., ed. Trace element geochemistry of volcanic rocks: Application for massive sulfide exploration: Geological association of Canada, short course notes: Vol. 12, pp. 79–173.

Pearce, J.A., 2008, Geochemical fingerprinting of oceanic basalts with applications to ophiolite classification and the search for Archean oceanic crust: Lithos, v. 100, p. 14–48. doi: 10.1016/j.lithos.2007.06.016

Pearce, J.A., and Stern, R.J., 2006, Origin of back-arc basin magmas: Trace element and isotope perspectives: Geophysical monograph: American Geophysical Union, v. 166, p. 63.

Pearce, J.A., Van De Lann, S.R., Arculus, R.J., Murton, B.J., Ishii, T., Peate, D.W., and Parkinson, I.J., 1992, Boninite and harzburgite from leg 125 (Bonin–Mariana forearc): A case study of magma genesis during the initial stage of subduction. In: Fryer, P., Pearce, J.A., and Stokking, L.B. (eds.), Bonin/Mariana Region. Proceedings of Ocean Drilling Program Leg, v. 125, p. 623–656.

Pearce, J., Barker, P., Edwards, S., Parkinson, I.J., and Leat, P.T., 2000, Geochemistry and tectonic significance of peridotites from the South Sandwich arc–basin system, South Atlantic: Contributions to Mineralogy and Petrology, v. 139, no. 1, p. 36–53. doi: 10.1007/s004100050572

Pedersen, R.B., and Malpas, J., 1984, The origin of oceanic plagiogranites from the karmøy ophiolite, western Norway: Contributions to Mineralogy and Petrology, v. 88, no. 1–2, p. 36–52. doi: 10.1007/bf00371410

Pressling, N., Morris, A., John, B.E., and MacLeod, C.J., 2012, The internal structure of an oceanic core complex: An integrated analysis of oriented borehole imagery from IODP Hole U1309D (Atlantis Massif): Geochemistry, Geophysics, Geosystems, v. 13, no. 9. doi: 10.1029/2012GC004061

Reagan, M.K., Ishizuka, O., Stern, R.J., Kelley, K.A., Ohara, Y., Blichert-Toft, J., Bloomer, S.H., Cash, J., Fryer, P., Hanan, B.B., Hickey-Vargas, R., Ishii, T., Kimura, J.I., Peater, D.W., Rowe, M. C., and Woods, M., 2010, Fore-arc basalts and subduction initiation in the Izu–Bonin–mariana system: Geochemistry Geophysics Geosystems, v. 11, p. Q03X12. doi: 10.1029/2009GC002871.

Ricou, L.E., Braud, J., and Brunn, J.H., 1977, Le Zagros, in Livre la M moire de Albert F. de Lapparent. Soc. G ol. rance, M moire hors-s rie: v. 8, p. 33–52.

Rollinson, H., 2017, Masirah – the other Oman ophiolite: A better analogue for mid-ocean ridge processes?: Geoscience Frontiers, v. 8, no. 6, p. 1253–1262. doi: 10.1016/j.gsf.2017.04.009

Rossetti, F., Monié, P., Nasrabady, M., Theye, T., Lucci, F., and Saadat, M., 2017, Early carboniferous subduction-zone metamorphism preserved within the Palaeo-Tethyan Rasht ophiolites (western Alborz, Iran): Journal of the Geological Society, v. 174, no. 4, p. 741–758. doi: 10.1144/jgs2016-130

Rubin, K.H., and Sinton, J.M., 2007, Inferences on mid-ocean ridge thermal and magmatic structure from MORB compositions, Earth Planet. Sci. Lett., v. 260, no. 1-2, p. 257–276. doi: 10.1016/j.epsl.2007.05.035

Saccani, E., Allahyari, K., Beccaluva, L., and Bianchini, G., 2013a. Geochemistry and petrology of the Kermanshah ophiolites (Iran): Implication for the interaction between passive rifting, oceanic accretion, and plume-components in the Southern Neo-Tethys Ocean: Gondwana Res., v. 24, p. 392–411. doi: 10.1016/j.gr.2012.10.009

Saccani, E., Allahyari, K., and Rahimzadeh, B., 2014, Petrology and geochemistry of mafic magmatic rocks from the SarveAbad ophiolites (Kurdistan region, Iran): Evidence for interaction between MORB-type asthenosphere and OIB-type components in the southern Neo-Tethys ocean: Tectonophysics, v. 621, p. 132–147. doi: 10.1016/j.tecto.2014.02.011

Saccani, E., Azimzadeh, Z., Dilek, Y., and Jahangiri, A., 2013b, Geochronology and petrology of the early carboniferous misho mafic complex (NW Iran), and implications for the melt evolution of Paleo-Tethyan rifting in Western Cimmeria: Lithos, v. 162–163, p. 264–278.

Saccani, E., Dilek, Y., and Photiades, A., 2018, Time-progressive mantle-melt evolution and magma production in a Tethyan marginal sea: A case study of the Albanide-Hellenide ophiolites: Lithosphere, v. 10, no. 1, p. 35–53. doi: 10.1130/L602.1

Saito, T., Uno, M., Sato, T., Fujisaki, W., Haraguchi, S., and Li, Y.B., 2015, Geochemistry of accreted metavolcanic rocks from the Neoproterozoic Gwna group of Anglesey-Lleyn, NW Wales, U.K.: MORB and OIB in the Iapetus ocean: Tectonophysics, v. 662, p. 243–255. doi: 10.1016/j.tecto.2015.08.015

Sapancı, Ö., Tokat, G., Eraslan, N.K., Karakaya, A.O., Gücer, M.A., and Çimen, O., 2023, Geochemical and radiometric data for mafic rocks from the Guleman ophiolite (SE, Turkey): New insights on the geodynamic evolution of the southern Neo-Tethyan ocean: Lithos, v. 442, no. 443, p. 107071. doi: 10.1016/j.lithos.2023.107071

Searle, M.P., Lippard, S.J., Smewing, J.D., and Rex, D.C., 1980, Volcanic rocks beneath the Semail ophiolite nappe in the northern Oman mountains and their significance in the Mesozoic evolution of Tethys: Journal of the Geological Society, v. 137, no. 5, p. 589–604. doi: 10.1144/gsjgs1375.0589

Sepidbar, F., Khedr, M.Z., Ghorbani, M.R., Palin, R.M., and Xiao, Y., 2021, Petrogenesis of arc-related peridotite hosted chromitite deposits in Sikhoran-Soghan mantle section, South Iran. Evidence for proto-forearc spreading to boninitic stages: Ore Geology Reviews, v. 136, p. 104256. doi: 10.1016/j.oregeorev.2021.104256

Sepidbar, F., Lucci, F., Biabangard, H., Zaki Khedr, M., and Jiantang, P., 2020, Geochemistry and tectonic significance of the Fannuj-Maskutan SSZ-type ophiolite (inner Makran, SE Iran): International Geology Review, v. 62, no. 16, p. 2077–2104. doi: 10.1080/00206814.2020.1753118

Seyfried, W.E., Berndt, M.E., and Seewald, J.S., 1988, Hydrothermal alteration processes at mid-ocean ridges: Constraints from diabase alteration experiments, hot-spring fluids and composition of the oceanic crust: Canadian Mineralogist, v. 26, p. 787–804.

Shervais, J.W., 1982, Ti-V plots and the petrogenesis of modern and ophiolitic lavas: Earth and Planetary Science Letters, v. 59, p. 101–118. doi: 10.1016/0012-821X(82)90120-0

Stern, R.J., 2004, Subduction initiation: Spontaneous and induced. Earth and Planetary Science Letters, v. 226, no. 3–4, p. 275–292. doi: 10.1016/j.epsl.2004.08.007

Stern, R.J., Reagan, M., Ishizuka, O., Ohara, Y., and Whattam, S., 2012, To understand subduction initiation, study forearc crust: To understand forearc crust, study ophiolites: Lithosphere, v. 4, no. 6, p. 469–483. doi: 10.1130/L183.1

Stöcklin, J., 1968, Structural history and tectonics of Iran; a review: AAPG Bulletin, v. 52, no. 7, p. 1229–1258. doi: 10.1306/5D25C4A5-16C1-11D7-8645000102C1865D

Sun, S.S., and McDonough, W.F., 1989, Chemical and isotopic systematics of oceanic basalt: Implications for mantle composition and processes LI ET AL. 17 and processes, *in* Saunders, A.D. and Norry, M.J., eds. Magmatism in the ocean basins: Special publication: London, Geological Society, Special Publication, Vol. 42, pp. 313–345.

Topuz, G., Çelik, Ö.F., Şengör, A.M.C., Altıntaş, İ.E., Zack, T., Rolland, Y., and Barth, M., 2013, Jurassic ophiolite formation and emplacement as backstop to a subduction-accretion complex in northeast Turkey, the Refahiye ophiolite, and relation to the Balkan ophiolites. American Journal of Science, v. 313, p.1054–1087. doi: 10.2475/10.2013.04

Warren, J.M., 2016, Global variations in abyssal peridotite compositions: Lithos, v. 248, p. 193–219. doi: 10.1016/j.lithos.2015.12.023

Whattam, S.A., and Stern, R.J., 2011, The 'subduction initiation rule': A key for linking ophiolites, intra-oceanic forearcs, and subduction initiation: Contributions to Mineralogy and Petrology, v. 162, p. 1031–1045. doi: 10.1007/s00410-011-0638-z

Whitechurch, H., Omrani, J., Agard, P., Humbert, F., Montigny, R., and Jolivet, L., 2013, Evidence for Paleocene–Eocene evolution of the foot of the Eurasian

margin (Kermanshah ophiolite, SW Iran) from back-arc to arc: Implications for regional geodynamics and obduction: Lithos, v. 182-183, p. 11–32. doi: 10.1016/j.lithos.2013.07.017

Winchester, J.A., and Floyd, P.A., 1977, Geochemical discrimination of different magma series and their differentiation products using immobile elements: Chemical Geology, v. 20, p. 325e343. doi: 10.1016/0009-2541(77)90057-2

Workman, R.K., and Hart, S.R., 2005, Major and trace element composition of the depleted MORB mantle (DMM): Earth and Planetary Science Letters, v. 231, no. 1–2, p. 53–72. doi: 10.1016/j.epsl.2004.12.005